

1 **Forecasting experiments of a dynamical-statistical model**
2 **of the sea surface temperature anomaly field based on the**
3 **improved self-memorization principle**

4 Mei Hong^{1,2}, Ren Zhang^{1,2}, Dong Wang³, Shuanghe Shen², Xi Chen¹, and
5 Vijay P. Singh⁴

6 ¹*Collaborative Innovation Center on Forecast and Evaluation of Meteorological Disaster, Nanjing University of*
7 *Information Science & Technology, Nanjing 210044, China*

8 ²*Institute of Meteorology and Oceanography, National University of Defense Technology, Nanjing 211101, China*

9 ³*Key Laboratory of Surficial Geochemistry, Ministry of Education; Department of Hydrosociences, School of Earth*
10 *Sciences and Engineering, Collaborative Innovation Center of South China Sea Studies, State Key Laboratory of*
11 *Pollution Control and Resource Reuse, Nanjing University, Nanjing 210093, China*

12 ⁴*Department of Biological and Agricultural Engineering, Zachry Department of Civil Engineering, Texas A & M*
13 *University, College Station, TX 77843, USA*

14
15
16 Corresponding authors address:

17 1. Ren Zhang, Research Centre of Ocean Environment Numerical Simulation,
18 Institute of Meteorology and Oceanography, National University of Defense
19 Technology, Nanjing 211101, China

20 E-mail: 254247175@qq.com

21 2. Xi Chen, Research Centre of Ocean Environment Numerical Simulation, Institute
22 of Meteorology and Oceanography, National University of Defense Technology,
23 Nanjing 211101, China

24 E-mail: chenxigfkd@163.com

25

26 **Abstract:** With the objective of tackling the problem of inaccurate long-term El Niño
27 Southern Oscillation (ENSO) forecasts, this paper develops a new
28 dynamical-statistical forecast model of sea surface temperature anomaly (SSTA) field.
29 To avoid single initial prediction values, a self-memorization principle is introduced
30 to improve the dynamic reconstruction model, thus making the model more
31 appropriate for describing such chaotic systems as ENSO events. The improved
32 dynamical-statistical model of the SSTA field is used to predict SSTA in the
33 equatorial eastern Pacific and during El Niño and La Niña events. The long-term
34 step-by-step forecast results and cross-validated retroactive hindcast results of time
35 series T_1 and T_2 are found to be satisfactory, with a pearson correlation coefficient of
36 approximately 0.80 and a mean absolute percentage error (MAPE) of less than 15%.
37 The corresponding forecast SSTA field is accurate in that not only is the forecast
38 shape similar to the actual field, but the contour lines are essentially the same. This
39 model can also be used to forecast the ENSO index. The temporal correlation
40 coefficient is 0.8062, and the MAPE value of 19.55% is small. The difference
41 between forecast results in spring and those in autumn is not high, indicating that the
42 improved model can overcome the spring predictability barrier to some extent.
43 Compared with six mature models published previously, the present model has an
44 advantage in prediction precision and length, and is a novel exploration of the ENSO
45 forecast method.

46

47 **Keywords:** Dynamical-statistical forecast model; self-memorization principle; sea

48 surface temperature field; long-term forecast of ENSO

49 **1. Introduction**

50 The El Niño Southern Oscillation (ENSO), the well-known coupled atmosphere
51 –ocean phenomenon, was firstly proposed by Bjerknes (1969). The ENSO
52 phenomenon can influences regional and global climates, so the prediction of ENSO
53 has received considerable public interest (Rasmusson and Carpenter, 1982; Glantz et
54 al., 1991).

55 Over the past two to three decades, one might reasonably expect the ability to
56 predict warm and cold episodes of ENSO at short and intermediate lead times to have
57 gradually improved (Barnston et al., 2012). Many countries have been focusing on
58 ENSO forecasts since the 1990s, and the ENSO forecast has become one of the
59 important research topics in the International Climate Change and Predictability
60 Research plan. The U.S. International Research Institute for Climate and Society, the
61 U.S. Climate Prediction Centre, Japan Meteorological Agency, and European Centre
62 for Medium-Range Weather Forecasting have developed different coupled
63 atmosphere–ocean models to forecast ENSO (Saha et al., 2006; Molteni et al., 2007) .

64 The forecast models can generally be divided into two types (Palmer et al., 2004).
65 The first type is typified by a dynamic model, which mathematically expresses
66 physical laws that govern how the ocean and the atmosphere interact. The second type
67 is typified by a statistical model, which requires large a amount of historical data and
68 analyses the data to do forecasting (Chen et al., 1995; Moore et al., 2006).

69 Over the past three decades, ENSO predictions have made remarkable progress,

70 reaching a stage where reasonable statistical and numerical forecasts (Jin et al.,
71 2008) can be made 6–12 months in advance (Wang et al., 2009a). . However, there are
72 three problems remaining to be resolved (Zhang et al., 2003a): (1) The current ENSO
73 predictions are mainly limited to the short term, such as annual and seasonal
74 predictions; (2) Although the representation of ENSO in coupled models has
75 advanced considerably during the last decade, several aspects of the simulated
76 climatology and ENSO are not well reproduced by the current generation of coupled
77 models. The systematic errors in SST are often very large in the equatorial Pacific,
78 and model representations of ENSO variability are often weak and/or incorrectly
79 located (Neelin et al. 1992; Mechoso et al. 1995; Delecluse et al. 1998; Davey et al.
80 2002). (3) Coupled models of ENSO predictions initialized from observed initial
81 states tend to adjust towards their own climatological mean and variability, leading to
82 forecast errors. The errors associated with such adjustments tend to be more
83 pronounced during boreal spring, which is often called the “spring predictability
84 barrier” (Webster et al., 1999). More efficient models are therefore desired (Belkin
85 and Niyogi, 2003; Weinberger and Saul, 2006). Therefore, the idea of combining
86 dynamical and statistical methods to improve weather and climate prediction has been
87 developed in many studies (Huang et al., 1993; Yu et al., 2014a; Yu et al., 2014b). By
88 introducing genetic algorithms (GAs), Zhang et al. (2006) inverted and reconstructed
89 a new dynamical-statistical forecast model of the tropical Pacific sea surface
90 temperature (SST) field using historic statistical data (Zhang et al., 2008). However,
91 there is one flaw in the forecast model: the time-delayed SST field. This is because

92 ENSO is a complicated system with many influencing factors. To overcome
93 information insufficiency in the forecast model, Hong et al. (2014) selected the
94 tropical Pacific SST, SSW and SLP fields as three modelling factors and utilized the
95 GA to optimize model parameters.

96 However, the above dynamical prediction equations which were ,proposed by
97 Hong et al.(2014), greatly depend on a single initial value, creating long-term
98 forecasts over 8 months that diverged significantly. These unsatisfactory results
99 indicate that this model needs to be improved. Cao (1993) first proposed the
100 self-memorization principle, which transforms the dynamical equations with the
101 self-memorization equations, wherein the observation data can determine the memory
102 coefficients. This method has been widely used in forecast problems in environmental,
103 hydrological and meteorological fields (Feng et al., 2001; Gu, 1998; Chen et al.,
104 2009). The method can avoid the question of initial conditions for the differential
105 equations, so it can be introduced here to improve the proposed dynamical forecast
106 model.

107 Therefore, an improved dynamical-statistical forecast model of the SST field
108 and its impact factors with a self-memorization function was developed. The
109 improved model can absorb the information from past observations.

110 This paper is organized as follows: Research data and forecast factors are
111 introduced in section 2. In Section 3 the reconstruction of the dynamical model of
112 SSTA field is described. To improve the reconstruction model, the self-memorization
113 principle is introduced in Section 4. Model forecast experiments are described in

114 Section 5, and conclusions are given in Section 6.

115 **2. Research data and forecast factors**

116 **2.1 Data**

117 The monthly average SST data were obtained from the UK Met Office Hadley
118 Centre for the region (30 °S-30 °N; 120 °E -90 °W). The gridded 1° × 1° Met Office
119 Hadley Sea Ice and SST dataset (HadISST1; Rayner et al. 2003) includes both in situ
120 and available satellite data. The sea areas provide important information on
121 ocean-atmosphere coupling in the East and West Pacific Ocean and the El Niño /La
122 Niña events. The reanalysis data, zonal winds and sea level pressures were obtained
123 from the National Center for Environmental Forecast of America and the National
124 Center for Atmospheric Research (Kalnay et al., 1996). The sea surface height (SSH)
125 field was obtained from Simple Ocean Data Assimilation (SODA) data (James and
126 Benjamin, 2008). Outgoing longwave radiation (OLR) was obtained from the
127 National Oceanic and Atmospheric Administration (NOAA) satellites, at a resolution
128 of 0.5° × 0.5° (Liebmann and Smith, 1996). The Southern Oscillation Index (SOI) data
129 were obtained from the Climate Prediction Center (CPC). The time series of all data
130 were from Jan. 1951 to Dec. 2010, 720 months in total.

131 **2.2 EOF deconstruction**

132 The sea surface temperature anomaly (SSTA) field can be calculated from the
133 SST field and can be deconstructed into time (coefficients)-space (structure) using the
134 empirical orthogonal function (EOF) method. Detailed information on the EOF
135 method can be seen in the related references (Dommenges & Latif, 2002). We have

136 used covariance matrix, because the covariance matrix was selected to diagnose the
137 primary patterns of co-variability in the basin-wide SSTs, rather than the patterns of
138 normalized covariance (or correlation matrix).

139 We used the smooths function with MATLAB to smooth the SSTA field before
140 the EOF deconstruction, which is five points two times moving, mainly filtering out
141 some noise points and outliers. Then an EOF analysis of smoothed anomalies was
142 performed, and the first two SSTA EOFs are shown in Figs. 1a and 1c. The principal
143 component (PC) time series corresponding to the first and second EOFs are shown in
144 Figs. 1b and 1d. The first EOF pattern, which accounted for 61.33% of the total SSTA
145 variance, represented the mature ENSO phase (El Niño or La Niña), and the
146 corresponding PC time series was highly correlated (with a correlation coefficient of
147 0.85) with the cold tongue index (SST anomaly averaged over 4°S – 4°N , 180° – 90°
148 W) over the whole period. The second EOF, accounting for 14.52% of the total
149 SSTA variance, indicated the ENSO signal beginning to enhance. Compared with the
150 first mode, these were slightly attenuated in terms of the scope and intensity. The
151 above analysis is similar to the EOF analysis of the SSTA field in the previous studies
152 (Johnson et al., 2000; Timmermann et al., 2001). This indicates that the front two
153 variance contribution modes can describe the main characteristics of the SSTA field
154 and El Niño/La Niña. Therefore, we can choose the T_1, T_2 time series EOF
155 decomposition modes as the modelling objects.

156 **2.3 Selection of other prediction model factors**

157 Considering the complexity of computation, the amount of variables in the

158 equations of our model can't be too large, usually 3 or 4 for the best. This has been
159 explained in our previous studies (Zhang et al., 2006; Zhang et al., 2008). If there are
160 more than 4 variables in the modeling equation, it will cause the amount of
161 parameters such as $a_1, a_2, \dots, a_n, b_1, b_2, \dots, b_n, \dots$ too large. The huge computation makes it
162 difficult to be precisely modeled. Thus, the total number of parameters in the model of
163 five variables was 102, which may cause an overfitting problem. Hence, when we
164 selected the model of five or six variables which entailed large amounts of
165 computation that made precision difficult, and too many parameters might cause an
166 overfitting phenomenon. If we choose only two or even fewer variables, the forecast
167 performance is poor too. Too few variables cause too small reconstructed parameters,
168 resulting in amounts of important information missing out in the model. Thus, four
169 variables are best for dynamically and accurately modeling. Because we have chosen
170 two time series in section 2.2 as the modeling objects, now we should select the other
171 two ENSO intensity impact factors.

172 The ENSO intensity impact factor is an important issue in ENSO prediction.
173 Previous studies have been completed in this area, which found that teleconnection
174 patterns, temperature, precipitation, wind and SSH may affect ENSO strength. For
175 example, Trenberth et al. (1998) noted that PNA, SOI and OLR in the Pacific
176 Intertropical Convergence Zone (ITCZ) are all closely related to ENSO.
177 Webster (1999) pointed out after the 1970, Indian Ocean dipole (IOD) is not only
178 affected by ENSO, but also affected the strength of ENSO (Ashok et al., 2001). Yoon
179 and Yeh (2010) reported that the Pacific Decadal Oscillation (PDO) disrupts the

180 linkage between El Niño and the following Northeast Asian summer monsoon
181 (NEASM) through inducing the Eurasian pattern in the mid-high latitudes. The vast
182 majority of studies (Tomita and Yasunari, 1996; Zhou and Wu, 2010; Kim et al., 2017)
183 have concentrated on the impacts of ENSO on the East Asian winter
184 monsoon(EAWM). During the EAWM season, ENSO generally reaches its mature
185 phase and has the most prominent impact on the climate. Wang et al. (1999a) and
186 Wang et al. (1999b) suggested that the zonal wind factors in the eastern and western
187 equatorial Pacific play a critical role in the phase of transition of the ENSO cycle,
188 which could excite eastward propagating Kelvin waves and affect the SSTA in the
189 equatorial Pacific. Zhao et al. (2012) analyzed the characteristics of the tropical
190 Pacific SSH field and its impact on ENSO events.

191 Based on the above analysis, we have selected nine factors, which may be
192 closely related with the ENSO index (Niño3.4).

193 (1)The zonal wind in the eastern equatorial Pacific factor (u_1) was calculated
194 as the grid-point average of zonal wind in the area [$5^\circ\text{S} \sim 5^\circ\text{N}$, $150^\circ\text{W} \sim 90^\circ\text{W}$].

195 (2) The zonal wind in the western equatorial Pacific factor (u_2) was calculated
196 as the grid-point average of zonal wind in the area [$0^\circ \sim 10^\circ\text{N}$; $135^\circ\text{E} \sim 180^\circ\text{E}$].

197 (3) The PNA teleconnection factor was obtained from the CPC.

198 (4) the dipole mode index factor (DMI) was obtained from SSTA for
199 June-July-August (JJA) based on Saji(1999) method.

200 (5) The SOI factor was obtained from the CPC.

201 (6) The PDOI factor was obtained from department of Atmospheric Sciences

202 in the university of Washington. The web is
203 <http://tao.atmos.washington.edu/pdo/RDO.latest>.

204 (7) The EAWM index (EAWMI) factor was proposed by Yang et al. (2002),
205 which is defined by the meridional 850-hPa winds averaged over the region (20°
206 $\sim 40^{\circ}$ N, $100^{\circ} \sim 140^{\circ}$ E).

207 (8) The OLR in the ITCZ factor was calculated as the grid-point average of
208 OLR in the area [10° N $\sim 20^{\circ}$ N, 120° E $\sim 150^{\circ}$ E].

209 (9) The SSH factor was calculated as the grid-point average of the SSH data in
210 the area [10° S $\sim 10^{\circ}$ N; 120° E $\sim 60^{\circ}$ W].

211 A correlation analysis of the above factors was carried out and the results are
212 shown in Table 1.

213 Table 1 shows that SOI and EAWMI have the stronger correlation with the
214 front two time series T_1, T_2 than the other 7 factors. The results are also consistent with
215 previous research (Clarke and Van Gorder, 2003; Drosowsky, 2006; Zhang et al.,
216 1996; Wang et al., 2008; Yang and Lu, 2014). Therefore, the first time series T_1 , the
217 second time series T_2 , SOI and EAWMI will be selected as prediction model factors.

218 **3. Reconstruction of dynamical model based on GA**

219 Takens' delay embedding theorem (Takens, 1981) provides the conditions under
220 which a smooth attractor can be constructed from observations made with a generic
221 function. Later results replaced the smooth attractor with a set of arbitrary
222 box-counting dimensions and the class of generic functions with other classes of
223 functions. Takens had shown that if we measured any single variable with sufficient

224 accuracy for a long period of time, it would be possible to construct the underlying
 225 dynamical structure of the entire system from the behavior of that single variable
 226 using delay coordinates and the embedding procedure. It was therefore possible to
 227 construct a dynamical model of system evolution from the observed time series.
 228 Introducing this idea here, four time series of the T_1 , T_2 , SOI and EAWMI factors
 229 were chosen to construct the dynamical model.

230 The basic idea of statistical-dynamical model construction is discussed in
 231 Appendix A and was introduced in our previous work (Zhang et al., 2006; Hong et al.,
 232 2014).

233 A simplified second-order nonlinear dynamical model can be used to depict the
 234 basic characteristics of atmosphere and ocean interactions (Fraedrich, 1987). Suppose
 235 that the following nonlinear second-order ordinary differential equations are taken as
 236 the dynamical model of reconstruction. In the equations, x_1, x_2, x_3, x_4 were used to
 237 represent the time coefficient series of T_1 , T_2 , SOI and EAWMI.

$$\begin{aligned}
 \frac{dx_1}{dt} &= a_1x_1 + a_2x_2 + a_3x_3 + a_4x_4 + a_5x_1^2 + a_6x_2^2 + a_7x_3^2 + a_8x_4^2 + a_9x_1x_2 + a_{10}x_1x_3 + a_{11}x_1x_4 + a_{12}x_2x_3 + a_{13}x_2x_4 + a_{14}x_3x_4 \\
 \frac{dx_2}{dt} &= b_1x_1 + b_2x_2 + b_3x_3 + b_4x_4 + b_5x_1^2 + b_6x_2^2 + b_7x_3^2 + b_8x_4^2 + b_9x_1x_2 + b_{10}x_1x_3 + b_{11}x_1x_4 + b_{12}x_2x_3 + b_{13}x_2x_4 + b_{14}x_3x_4 \\
 \frac{dx_3}{dt} &= c_1x_1 + c_2x_2 + c_3x_3 + c_4x_4 + c_5x_1^2 + c_6x_2^2 + c_7x_3^2 + c_8x_4^2 + c_9x_1x_2 + c_{10}x_1x_3 + c_{11}x_1x_4 + c_{12}x_2x_3 + c_{13}x_2x_4 + c_{14}x_3x_4 \\
 \frac{dx_4}{dt} &= d_1x_1 + d_2x_2 + d_3x_3 + d_4x_4 + d_5x_1^2 + d_6x_2^2 + d_7x_3^2 + d_8x_4^2 + d_9x_1x_2 + d_{10}x_1x_3 + d_{11}x_1x_4 + d_{12}x_2x_3 + d_{13}x_2x_4 + d_{14}x_3x_4
 \end{aligned}
 \tag{1}$$

241 Based on the parameter optimization search method of GA in Appendix A, the
 242 time coefficient series of T_1 , T_2 , SOI and EAWMI from January 1951 to April 2008

243 are chosen as the expected data to optimize and retrieve model parameters. In order to
 244 eliminate the dimensionless relationship between variables, data standardization is to
 245 transform data from different orders of magnitude to the same order of magnitude,
 246 thus making the data comparable. So we used $x_{nor} = \frac{x - x_{min}}{x_{max} - x_{min}}$ to normalize the raw
 247 value of each of the four predictors, then we used the normalized value to model and
 248 forecast. Finally, we made forecast results revert back to the raw data magnitude by
 249 $x = x_{nor}(x_{max} - x_{min}) + x_{min}$.

250 In order to quantitatively compare the relative contribution of each item of our
 251 model to the evolution of the system, we calculated the relative variance contribution.

252 The formula is as follows: $R_i = \frac{1}{n} \sum_{j=1}^n [\frac{T_i^2}{\sum_{i=1}^{14} T_i^2}]$, $i = 1, 2, \dots, 14$, Where n is the length of

253 the data, $T_i = a_1x_1, a_2x_2, \dots, a_{14}x_3x_4$ is the item in the equation. According to our
 254 previous research (Hong et al., 2007), the variance contribution of the real item
 255 reflecting the performance of the model has a large proportion, while the variance
 256 contribution of the false term is almost zero, so we delete the weak items of
 257 $R_i < 0.01$.

258 After deleting the weak items, the nonlinear dynamical model of the first time
 259 series T_1 , the second time series T_2 , SOI and EAWMI can be reconstructed as follows:

$$\begin{aligned}
 \frac{dx_1}{dt} &= F_1 = -0.3328x_1 + 1.2574x_2 - 0.3511x_3 - 0.0289x_1^2 + 3.1280x_3^2 + 0.0125x_1x_2 + 2.7805x_1x_3 - 1.5408x_2x_4 \\
 \frac{dx_2}{dt} &= F_2 = 1.0307x_1 - 3.1428x_2 + 0.3095x_4 + 4.2301x_1^2 - 1.2066x_2^2 + 2.5024x_4^2 - 0.2891x_1x_3 + 0.7815x_1x_4 - 0.4266x_3x_4 \\
 \frac{dx_3}{dt} &= F_3 = -2.3155x_1 + 3.2166x_3 + 1.5284x_4 - 1.4527x_2^2 - 0.0034x_3^2 - 4.1206x_4^2 - 0.0025x_1x_4 + 0.0277x_2x_3 + 1.2860x_2x_4 \\
 \frac{dx_4}{dt} &= F_4 = 0.4478x_2 - 0.0268x_4 + 0.8995x_1^2 - 2.3890x_3^2 + 0.2037x_4^2 + 1.3035x_1x_2 + 2.0458x_1x_4 - 2.0015x_2x_4
 \end{aligned}$$

261 (2)

262 The model required testing. Because the training period was from January 1951
263 to April 2008, we chose T_1 , T_2 , SOI and EAWMI of May 2008, which were not used
264 as initial forecast data in the modeling. Next, the Runge–Kutta method was used to do
265 the numerical integration of the above equations, and every step of the integration was
266 regarded as 1 month's worth of forecasting results. As a result, forecast results of four
267 time series over a period of 20 months were obtained. Here, the focus was on the
268 forecast results of T_1 and T_2 , as shown in Fig.2.

269 The Pearson correlation coefficient (CC) (Wang et al. 2009b) and the mean
270 absolute percentage error (MAPE) (Hu et al. 2001) are employed as objective
271 functions to calibrate the model. The CC evaluates the linear relationship between the
272 observed and predicting values and MAPE measures the difference between the
273 observed and predicting values.

274 From Fig. 2, forecast performance of T_1 and T_2 within 5 months was better.
275 Using T_1 as an example, the CC between model predictions and corresponding
276 observations over the first five months forecasts was 0.8966 and MAPE was 8.32%.
277 However, after 5 months, MAPE increased rapidly, and was 31.29% at 10 months.
278 The model forecast then significantly diverged from observations, and the forecast
279 became inaccurate. After 10 months, the forecast results became increasingly worse,
280 which indicated that the forecast of the model after 5 months was unacceptable. The
281 forecast results of T_2 were similar to those of T_1 .

282 The model's skill should be further assessed by cross-validated retroactive
283 hindcasts of the time series. As in the above example, omitting a portion of the time

284 series (12 months, Jan. 1951 to Dec. 1951) from observations, we trained the model
285 based on the data from Jan. 1951 to Dec. 2010, and then predicted the omitted
286 segments (12 months, Jan. 1951 to Dec. 1951). Then in the next prediction
287 experiment, the omitted segment is Jan.1952 to Dec. 1952 and the training samples
288 are Jan. 1951 to Dec.1951 and Jan.1953 to Dec.2010. So the forecast time series is
289 Jan.1952 to Dec. 1952.We then repeated this procedure by moving the omitted
290 segment along the entirety of the available time series. Each experiment has used the
291 different training sample and have established the different model equation (but the
292 method is the same). The similar process of the cross-validated retroactive hindcasts
293 has also been used in the previous literatures (Hu et al., 2017).

294 Finally, we obtained cross-validated retroactive hindcast results of T_1 and T_2 , as
295 shown in Fig. 3. So the forecast results of 60 cross experiment (each experiment is the
296 prediction of the 12 month as Fig.2) according to the time sequence can merger into a
297 new time series (from Jan.1951-Dec.2010), and then the pearson correlation
298 coefficient (CC) and the mean absolute percentage error (MAPE) can be calculated by
299 the new prediction time series and the time series of the actual value. Figure 3 is
300 combined results of the 60 forecast experiments.

301 As Fig. 2, the forecast performance of T_1 and T_2 in Fig. 3 was not satisfactory.
302 The model forecast significantly diverged from observations, and the forecast became
303 inaccurate. The CC of T_1 and T_2 between model predictions and corresponding
304 observations were 0.3411 and 0.4176, respectively. Additionally, the MAPE of T_1 and
305 T_2 were 65.42% and 57.56%, respectively. This indicates that the forecast of the model
306 in the long -term was inaccurate and unacceptable.

307 The forecast result may be inaccurate when the integral forecasting time is long.
308 There will be a significant divergence which will cause an ineffective forecast. To
309 improve the forecast accuracy, the forecast not only depends on the integral equation
310 but also on a single initial value. Choosing the different initial value will cause
311 different forecast accuracy. For example, in a total of 60 cross-validated retroactive
312 hindcasts examples, the minimum MAPE was 37.65%, while the maximum MAPE
313 was 89.88%. A forecast, depending on a single initial value, will cause instability of
314 the forecast results. These two problems are addressed by introducing the
315 self-memorization principle in the next section.

316

317 **4. Introduction of self-memorization dynamics to improve the** 318 **reconstructed model**

319 In the above discussion, it was shown that the accuracy of the forecast results of
320 equation (2) were unsatisfactory. To improve long-term forecasting results, the
321 principle of self-memorization can be introduced into the mature model (Gu, 1998;
322 Chen et al., 2009). The principle of self-memorization dynamics (Cao, 1993; Feng et
323 al., 2001) can be seen in Appendix B.

324 Based on Eq. (B10) in Appendix B, the improved model can be expressed as

$$\text{325 follows: } \left\{ \begin{array}{l} x_{1t} = \sum_{i=-p-1}^{-1} \alpha_{1i} y_{1i} + \sum_{i=-p}^0 \theta_{1i} F_1(x_{1i}, x_{2i}, x_{3i}, x_{4i}) \\ x_{2t} = \sum_{i=-p-1}^{-1} \alpha_{2i} y_{2i} + \sum_{i=-p}^0 \theta_{2i} F_2(x_{1i}, x_{2i}, x_{3i}, x_{4i}) \\ x_{3t} = \sum_{i=-p-1}^{-1} \alpha_{3i} y_{3i} + \sum_{i=-p}^0 \theta_{3i} F_3(x_{1i}, x_{2i}, x_{3i}, x_{4i}) \\ x_{4t} = \sum_{i=-p-1}^{-1} \alpha_{4i} y_{4i} + \sum_{i=-p}^0 \theta_{4i} F_4(x_{1i}, x_{2i}, x_{3i}, x_{4i}) \end{array} \right. \quad (3)$$

326 where y_i is replaced by the mean of two values at adjoining times; i.e.,
 327 $y_i \equiv \frac{1}{2}(x_{i+1} + x_i)$; F is the dynamic core of the self-memorization equation, which
 328 can be obtained from Eq. (2); and α and θ are the memory coefficients, the formula
 329 for which can be found in Appendix B.

330 If the values of α and θ can be obtained, Eq. (3) can be used to obtain the
 331 results of final prediction. The memory coefficients α and θ in Eq. (3) were
 332 calibrated using the least-squares method with the same data (January 1951 to April
 333 2008) as those used in Section 3. Eq. (3) can be deconstructed as follows (M is the
 334 length of the time series):

$$335 \quad X = \begin{bmatrix} x_{11} \\ x_{12} \\ \cdot \\ \cdot \\ \cdot \\ x_{1M} \end{bmatrix}, \alpha = \begin{bmatrix} \alpha_{-p-1} \\ \alpha_{-p} \\ \cdot \\ \cdot \\ \cdot \\ \alpha_{-1} \end{bmatrix}, Y = \begin{bmatrix} y_{-p-1,1} & y_{-p,1} & \cdots & y_{-1,1} \\ y_{-p-1,2} & y_{-p,2} & \cdots & y_{-1,2} \\ \cdot & \cdot & & \cdot \\ \cdot & \cdot & & \cdot \\ \cdot & \cdot & & \cdot \\ y_{-p-1,M} & y_{-p,M} & \cdots & y_{-1,M} \end{bmatrix}, \Theta = \begin{bmatrix} \theta_{-p} \\ \theta_{-p+1} \\ \cdot \\ \cdot \\ \cdot \\ \theta_0 \end{bmatrix},$$

$$336 \quad F = \begin{bmatrix} F_{-p,1} & F_{-p+1,1} & \cdots & F_{0,1} \\ F_{-p,2} & F_{-p+1,2} & \cdots & F_{0,2} \\ \cdot & \cdot & & \cdot \\ \cdot & \cdot & & \cdot \\ \cdot & \cdot & & \cdot \\ F_{-p,M} & F_{-p+1,M} & \cdots & F_{0,M} \end{bmatrix}$$

337 The matrix equation is:

$$338 \quad X = Y\alpha + F\theta \quad (4)$$

$$339 \quad \text{where } Z = [Y; F], \quad W = \begin{bmatrix} \alpha \\ \cdot \\ \cdot \\ \Theta \end{bmatrix}.$$

340 Eq. (4) can be written as:

341
$$X = ZW \tag{5}$$

342 The memory coefficients vector W can be calibrated using the least squares
 343 method:

344
$$W = (Z^T Z)^{-1} Z^T X \tag{6}$$

345 The memory coefficients a, θ can be obtained from Eq. (6). We then made a
 346 prediction using the self- memorization equation (3), which used the p values before
 347 t_0 .

348 The coefficients in F and W were used with the same training data from January
 349 1951 to April 2008. In the forecast examples, we trained both the coefficients in F and
 350 W at the same time, but in the paper we describe them separately to facilitate the
 351 reader for better understanding.

352 **5. Model prediction experiments**

353 **5.1 Forecast of time series T_1 and T_2**

354 The training sample for the model was from January 1951 to April 2008. Here, from
 355 Eq. (3), the forecast results using T_1, T_2 , SOI and EAWMI factors can be calculated, called
 356 as step-by-step forecast.

357 When the retrospective order p is confirmed, step-by-step forecasts can be
 358 carried out. For example, when the T_1, T_2 , SOI and EAWMI values of May 2008 were
 359 forecast, y_i was obtained from the previous $p + 1$ time of T_1, T_2 , the SOI and the
 360 EAWMI data, and $F_i(x_{1i}, x_{2i}, x_{3i}, x_{4i})$ was obtained from the previous p times of
 361 T_1, T_2 , the SOI and the EAWMI data. All four equations were integrated simultaneously.
 362 Taking these in Eq. (3), we can get the T_1, T_2 , SOI and EAWMI values of May 2008,

363 which these can be taken as the initial values for the next prediction step. Then, the
364 T_1, T_2 , SOI and EAWMI values from June 2008 and so on, can be generated.

365 5.1.1 Determination of p

366 Based on the self-memorization principle, the self-memorization of the system
367 determines the retrospective order p (Cao, 1993). If the system forgets slowly,
368 parameters a and θ will be small and the p value should be high. The SSTA field
369 forecasts were on a monthly scale, the change of which was slow in contrast to
370 large-scale atmospheric motion. So parameters a and θ were small, and generally,
371 the p value was in the range 5 to 15.

372 The retrospective order p was obtained by a trial calculation method. We selected
373 the p values in the range 4 to 16 to construct the model. The CC and MAPE of
374 long-term fitting test (from February 1951 to December 2010) are shown in Table 2,
375 which can be used as the standard to determine the retrospective order p .

376 Table 2 indicates that when $p = 6$, the MAPE values of long-term fitting test
377 were the smallest and the CCs were the largest. Also, when p from 5 to 9, The CCs
378 were all more than 0.58 and the forecast results were all good, which is consistent
379 with our interpretation of the physical mechanisms in section 6.2 below. SOI and
380 EMWMI were 5-12 months lead relationships with SST (Xu et al., 1993; Chen et al,
381 2010; Wang et al., 2003). Using a cumulative period of SOI, EMWMI 5-8 months
382 ahead as initial values can help improve the final forecast results. Our results in table
383 2 are consistent with the actual physical ENSO process. Therefore, we selected the
384 retrospective order as $p=6$.

385 Then, the prediction experiments can be carried out, based on improved
 386 self-memorization Eq. (3).

387 The improved self-memorization equation of T_1, T_2 , SOI and EAWMI can then be
 388 established. After the differential equation was discretely dealt with, the memory
 389 coefficients were solved by the least-squares method given in section 4 (Training
 390 period is January 1951 to April 2008). Finally, the improved prediction equation of
 391 T_1, T_2 , SOI and EAWMI, based on the self-memorization principle, can be expressed
 392 as:

$$\begin{cases}
 x_{1t} = \sum_{i=-7}^{-1} \alpha_{1i} y_{1i} + \sum_{i=-6}^0 \theta_{1i} F_1(x_{1i}, x_{2i}, x_{3i}, x_{4i}) \\
 x_{2t} = \sum_{i=-7}^{-1} \alpha_{2i} y_{2i} + \sum_{i=-6}^0 \theta_{2i} F_2(x_{1i}, x_{2i}, x_{3i}, x_{4i}) \\
 x_{3t} = \sum_{i=-7}^{-1} \alpha_{3i} y_{3i} + \sum_{i=-6}^0 \theta_{3i} F_3(x_{1i}, x_{2i}, x_{3i}, x_{4i}) \\
 x_{4t} = \sum_{i=-7}^{-1} \alpha_{4i} y_{4i} + \sum_{i=-6}^0 \theta_{4i} F_4(x_{1i}, x_{2i}, x_{3i}, x_{4i})
 \end{cases} \quad (7)$$

394 where

$$\alpha = [\alpha_{ij}] = \begin{bmatrix} 0.0315 & -2.113 & 0.0284 & 2.1468 & 0.0688 & -0.7014 & 1.3248 \\
 0.4088 & -1.887 & -1.0233 & 1.5485 & 0.9028 & 1.0255 & -0.6443 \\
 -0.9088 & -0.2557 & 0.9671 & -0.0054 & 1.0568 & 2.9764 & -0.5234 \\
 0.2088 & -1.0567 & 0.4891 & -0.5066 & -0.4890 & 1.4555 & 1.0966 \end{bmatrix}$$

$$(i = 0, 1, \dots, 4; j = -7, -6, \dots, -1)$$

$$\theta = [\theta_{ij}] = \begin{bmatrix} 0.0485 & 0.0425 & -1.7688 & 0.8543 & 2.8901 & -0.1788 & -0.9066 \\
 0.07642 & 0.0941 & -1.2466 & -0.2288 & 0.1097 & 2.3221 & -1.4228 \\
 -0.5288 & 1.2368 & -0.5568 & -0.0155 & 0.2886 & -0.1560 & 1.2775 \\
 1.5335 & -0.2887 & -0.5336 & -0.6072 & -0.5611 & 1.0225 & -1.0625 \end{bmatrix}$$

$$(i = 0, 1, \dots, 4; j = -6, -5, \dots, 0)$$

397 The step-by-step forecast was performed. The retrospective order $p = 6$ means
 398 that earlier seven observation data ($p + 1 = 7$) should be used during the forecasting
 399 process. The forecast results per month were saved for the next period predictions.

400 5.1.2 Long-term step-by-step forecasts of T_1 and T_2

401 To test the actual forecast performance of the above improved model, long-term
402 step-by-step forecasts of T_1 and T_2 from May 2008 to December 2010 for 20 months
403 were carried out, as shown in Fig. 4. The forecast results of T_1 and T_2 were good.
404 Within 8 months, the CCs of T_1 and T_2 were 0.9163 and 0.9187. MAPEs of T_1 and
405 T_2 were small, only 5.86% and 6.78%. The forecast time series from 8 months to 14
406 months gradually diverged, but the trend was acceptable. The CCs of T_1 and T_2
407 reached 0.8375 and 0.8251, and MAPEs of T_1 and T_2 were 8.32% and 9.11%. After
408 14 months, forecast began to diverge and the error started to increase, but the CCs of
409 T_1 and T_2 remained about 0.6899 and 0.6782, and MAPEs reached 18.31% and
410 19.44%, which can be acceptable.

411 **5.2 Cross-validated retroactive hindcasts of time series T_1 and T_2**

412 As in section 3, the model's skill should be further assessed by cross-validated
413 retroactive hindcasts of the time series. Because our step-by-step forecasts need the
414 earlier seven observation data ($p + 1 = 7$), we can obtain cross-validated retroactive
415 hindcast results of T_1 and T_2 from August 1951 to December 2010, as shown in Fig.
416 5.

417 From Fig. 5, the forecast performance of T_1 and T_2 was good. The CCs of
418 T_1 and T_2 were 0.7124 and 0.7036, respectively. The MAPEs of T_1 and T_2 were
419 small, only 19.57% and 19.79%, respectively. The peaks and valleys of T_1 and T_2
420 were also forecasted accurately. The forecast results indicated that the cross-validated
421 retroactive hindcast results of T_1 and T_2 were close to the observed values.

422 Compared to Fig. 3, the improved model had better forecast abilities than the original
423 model.

424 Many researchers (Zhang et al., 2003b; Smith, 2004) have used Oceanic Niño
425 Index (ONI) which is used by the U.S. NOAA Climate Prediction Center to determine
426 the El Niño and La Niña years. It defined that the ONIs of five consecutive months in
427 winter were all more than 0.5 (less than -0.5) is the ElNiño (La Niña) year. Based on
428 the above criterion, we can divide the total 60 years (1951-2010) into three categories.
429 It includes the 18 examples of ElNiño year (such as 1958, 1964, 1966, etc.), 22
430 examples of LaNiña year (such as 1951, 1955, 1956, etc.) and the remaining 20
431 experiments of the neutral year. Since the details in Fig.5 is not clear, we list the
432 forecast results of 60 experiments (including 18 El Niño examples, 22 La Niña
433 examples and 20 Neutral examples) in table 3.

434 From table 3, the average of CC of both T_1 and T_2 of 60 experiments within
435 6 months was more than 0.84 and MAPE was less than 8%. The average of CC within
436 12 months was more than 0.74 and MAPE was less than 12%. According to the
437 literature (Barranel et al., 1999), when MAPE was less than 15%, which means the
438 error was not great and the forecast results were good. Obviously, the forecast results
439 of ElNiño / LaNiña experiments were a little worse than those of neutral examples,
440 which means the forecast ability of our model for the abnormal situation was a little
441 worse than those for the normal situation. But even for ElNiño / LaNiña experiments,
442 the average of CC was still more than 0.7 and MAPE was less than 15%, which
443 means the error was not too large and was still within an acceptable range.

444 **5.3Forecast of the SSTA field**

445 When we obtained the forecast results of the time coefficient series T_1 and T_2 ,
446 we submitted them into the following equation to reconstruct the forecast SSTA field:

$$447 \quad \hat{x}_t = \sum_{n=1}^2 E_n \bullet T_m, t=1,2,\dots,12 \quad (8)$$

448 where E_n , T_m are the EOF space fields and forecast time coefficients,
449 respectively, and \hat{x}_{ij} is the forecast SSTA field reconstructed by EOF.

450 After reconstruction of the space mode (treated as constant) and time coefficient
451 series (model prediction), the forecast of the SSTA fields was obtained, based on the
452 forecast results of T_1 and T_2 in Section 5.2. For economy of space, we cannot draw
453 all of the forecasted SSTA fields, so we selected a strong El Niño event (December
454 1997), a strong La Niña event (December 1999) and a neutral event (November 2002)
455 as examples.

456 Fig. 6 shows the forecast SSTA field during a strong El Niño event. From the
457 actual SSTA field in December 1997 (Fig. 6a), an obvious warm tongue structure
458 occurred in the area of [10°S~5°N, 90°W~150°W] in the Eastern Equatorial Pacific,
459 and a warm anomalous distribution arose in the west Pacific, which indicated a weak
460 El Niño event. The forecasted SSTA field of December 1997 is shown in Fig. 6b.
461 Although the range of warm tongue was a little bigger than the actual situation, the
462 forecast shape was similar to the actual field and also the contour lines were similar.
463 The average MAPE between the forecast field and the actual field is 8.56%, which
464 was controlled within 10%. The forecast results of the improved model event were
465 quite good for the El Niño event.

466 Fig.7 shows the forecasted SSTA field of a strong La Niña event. From the actual

467 SSTA field in December 1999 (Fig. 7a), an obvious cold pool occurred in the area of
468 [10 °S~10 °N, 120 °W~180 °W] in the Equatorial Pacific, which covered the Niño3.4
469 area. This SSTA field presented a strong strength La Niña event. The forecast SSTA
470 field from December 1999 is shown as Fig. 7b. Although the strength of the cold pool
471 was weaker than the actual situation, the forecast shape was similar to that of the
472 actual field. The average MAPE between the forecast field and the actual field was
473 9.69%. The errors were larger than that of the El Niño event, but they can be
474 controlled within 10%, which is acceptable.

475 Fig. 8 shows the forecasted SSTA field of a neutral event. From the actual SSTA
476 field in November 2002 (Fig. 8a), a warm pool occurred in the area of [10 °S~10 °N,
477 120 °W~180 °W] in the Equatorial Pacific, which covered the Niño3.4 area. However,
478 the warm pool was small and weak, which represented a neutral event. The forecasted
479 SSTA field from November 2002 is shown in Fig. 8b. Comparing Figures 6, 7 and 8,
480 we can see that the forecasted SSTA field of a neutral event was a little worse than
481 that of the El Niño and La Niña events. The forecasted shape of the SSTA field
482 basically described the actual situation, but the warm pool in the Niño3.4 area was
483 stronger and bigger than that of the actual situation, which indicated a borderline El
484 Niño event. The average MAPE between the forecasted field and the actual field was
485 14.50%, which was big but can be accepted.

486 We obtained the average values of MAPE of 18 El Niño events, 22 La Niña
487 events and 20 neutral events, which were 9.52%, 9.88% and 14.67%, respectively,
488 representing a good SSTA field forecasting ability of our model.

489 **5.4 Forecast of ENSO index**

490 The ENSO index can be represented as the sea surface temperature anomaly
491 (SSTA) in the Niño-3.4 region (5°N - 5°S , 120° - 170°W) and the ENSO index
492 forecast was the 3-month forecast (Barnston et al. 2012). So we also can pick up the
493 ENSO index from the above forecasted SSTA field. The forecast results of the ENSO
494 index within 20 months can also be obtained. The definition of lead time can be seen
495 in the reference (Barnston et al. 2012). Therefore, similar to the forecast experiment in
496 section 5.1, a succession of running 3-month mean SST anomalies with respect to the
497 climatological means for the respective prediction periods, averaged over the Niño 3.4
498 region, can be obtained, as demonstrated in Fig. 9.

499 The evaluation criteria of the ENSO index is the temporal correlation (TC), its
500 definition and specific calculation steps can be seen in these literatures (Kathrin et
501 al.,2016; Nicosia et al. 2013); The TC is often used to measure the prediction effect of
502 the ENSO index. For example, Barnston et al.in 2012 also used the TC to compare the
503 forecast skill of 21 real-time seasonal ENSO models.

504 The forecast results within lead times of 18 months are shown in Fig. 9, which
505 demonstrate that the forecast results of the ENSO index are good. Within lead time of
506 12 months, the TC was 0.8985 and the MAPE value was small, only 8.91%. In
507 addition, the borderline La Niña event in 2008–2009 was predicted well. After lead
508 times of 12 months, forecasts began to diverge and the errors started to increase.
509 Although the TC remained approximately 0.61, MAPE reached 18.58%. Therefore, a
510 moderate strength El Niño event that occurred in 2009/10 was not predicted.

511 We should give more examples to test the ENSO prediction ability of our model.
512 As in section 5.3, we can divide 60 examples as three types, which are examples of
513 ElNiño year, LaNiña year and neutral year. Finally, we can obtain the forecast results
514 of different types of examples in different lead times, as shown in table 4.

515 From table 4, the average TC of 60 experiments was 0.712 and the average
516 MAPE was 7.62% within 12 months for all seasons of lead time, which indicates that
517 the overall ENSO forecast ability of our model was good. The forecast results of the
518 El Niño examples were significantly worse than those of La Niña examples, while the
519 forecast results of La Niña examples were significantly worse than those of neutral
520 examples, which show the model forecast ability of the abnormal state was worse than
521 the normal state of the ENSO index. Even for the forecast results of El Niño examples,
522 the average TC was still above 0.6 and the average MAPE can be controlled below
523 10%, which means the forecast results were still in the acceptable range. Our model
524 not only accurately predicted the stronger El Niño and La Niña phases but also the
525 neutral states.

526 The ENSO forecast often had a spring predictability barrier (Webster, 1999),
527 which was most prominent during decades of relatively poor predictability
528 (Balmaseda et al., 1995). To test our model, the skill should be computed over the
529 entire time series and separately for seasonal subsets of the time series. From the
530 table4, we can see that although the forecast results of the present model in the spring
531 were worse than in the autumn, the margin was not high, which means the model can
532 overcome the “spring predictability barrier,” to some extent.

533 **5.5 Compared with six mature models**

534 Barnston et al. (2012) compared many ENSO forecast models. Based on his
535 research, we selected four high quality dynamical models, including ECMWF, JMA,
536 the National Aeronautics and Space Administration Global Modelling and
537 Assimilation Office (NASAGMAO) and the National Centre for Environmental
538 Prediction Climate Forecast System (NCEP CFS; Version1). Two high quality
539 statistical models also be selected, including the University of California, Los Angeles
540 Theoretical Climate Dynamics (UCLA-TCD) multilevel regression model and the
541 NOAA/NCEP/CPC constructed Analogue (CA) model. The detail of the above
542 models can be seen in these references (Reynolds al., 2002; Luo et al., 2005; Barnston
543 et al., 2012).

544 We then compared the forecast ability of the above six models with that of our
545 model. All of the experiments of our model and six other models were conducted
546 under the same conditions using the same historical data for modelling and the same
547 initial values to forecast. In the CPC website, there are detailed explanations of six
548 models' training samples and the initial values. So we do not need to install all these
549 models on their own machines and run them for forecasting. We just made training
550 samples and initial values of our model were the same with those of selected six
551 models. At an 8-month lead time, the TC of our model for all seasons combined was
552 0.613 (Fig. 10). In brief, the forecast ability of the ECMWF model was slightly better
553 than that of our model but the ability of the other 5 models was worse than that of our
554 model. While, in regard to the forecast length, the TC within 12 months of our model

555 is greater than 0.6, which was superior to the ECMWF model. In addition, the forecast
556 results of the UCLA-TCD model and the CPC CA model reduced quickly after
557 5-month lead times, so the forecast ability of our model was more stable than them.

558 The root mean square error (RMSE) was also examined to assess the
559 performance of discrimination and calibration. Barnston et al. (2012) believed that all
560 seasonal RMSE values contributed equally to a seasonally combined RMSE. So we
561 drew figure 11 to show seasonally combined RMSE.

562 From Fig. 10 and Fig. 11, we can see the highest correlation tend to have
563 lower RMSE. So the RMSE of our model was slightly higher than that of ECMWF
564 model, but it was much lower than those of the other 5 models. Figure 11 and Figure
565 12 is the average TC and RMSE of the 240 experiments of compared with six mature
566 models, covers a variety of different types of ENSO and different lead time. So those
567 samples should be really representative.

568 **6. Conclusions and discussion**

569 **6.1 Conclusions**

570 A new forecasting model of the SSTA field was proposed based on a dynamic
571 system reconstruction idea and the principle of self-memorization. The approach of
572 the present paper consisted of the following steps:

573 (1) The SST field can be time (coefficients)-space (structure) deconstructed
574 using the EOF method. Take T_1 , T_2 , SOI and EAWMI and consider them as
575 trajectories of a set of four coupled quadratic differential equations based on the
576 dynamic system reconstruction idea. The parameters of this dynamic model were

577 estimated using a GA.

578 (2) The forecast results of the dynamic model can be improved by the
579 self-memorization principle. The memory coefficients in the improved
580 self-memorization model were obtained using the GA method.

581 (3) The long-term step-by-step forecast results and cross-validated
582 retroactive hindcast results of time series T_1 and T_2 are all found to be good, with the
583 CC of approximately 0.80 and the MAPE of less than 15%.

584 (4) The improved model was used to forecast the SSTA field. The
585 forecasted SSTA fields of three types of events are accurate. Not only is the forecast
586 shape similar to the actual field but also the contour lines are similar.

587 (5) The improved model was also used to forecast the ENSO index. The
588 average TC of 60 examples within 12 months is 0.712, and the MAPE value is small,
589 only 7.62%, which proves that the improved model has better forecasting results of
590 the ENSO index. Although the forecast results of the model in the summer were
591 worse than in the winter, the margin was not high, which means that the model can
592 overcome the spring predictability barrier to some extent. Finally, compared with the
593 six mature models, the new dynamical-statistical forecasting model has a scientific
594 significance and practical value for the SST in the eastern equatorial Pacific and El
595 Niño/La Niña event predictions.

596 **6.2 Discussion**

597 L'Heureux et al.(2013) reported that using different data sets and time periods,
598 the 2nd EOF is not stable, being entirely due to the strong trend. So we need to do

599 more experiments to prove that we choose the second mode of EOF to be appropriate,
600 and whether different time periods will make us forecast unstable or not. Our original
601 data is the monthly average SST data from January 1951 to Dec. 2010, which are 60
602 years. We will increase the length of the data for 20 years (Jan.1931 –Dec.2010), for
603 10 years (Jan.1941- Dec.2010) and decrease the length of the data for 10 years
604 (Jan.1961- Dec.2010), for 20 years (Jan.1971- Dec.2010). And then we use the same
605 method to reconstruct a model and forecast the ENSO index as section5.4. The
606 prediction results are shown in the table5.

607 From the table, we can see that in the 60 experiments, the prediction results of
608 the data period increased by 20 years are the best, and the prediction results of the
609 data period decreased by 20 years is the worst. This is because the more data we use,
610 the more information it contain. But from the table we can also see the difference
611 among forecast results of both TC and MAPE of five different sample data are less,
612 and no abnormal change suddenly worse or better appear. All these indicate that using
613 different data sets and time periods, even though may have a certain impact on the
614 pattern of the 2nd EOF, but the impact on our forecast is not great and it will not
615 make our forecast unstable.

616 Actually, how many variables and which variables are used in our model
617 become a key issue to be resolved. We are a complex four factor differential
618 equations coupling model. We are a complex coupled model of four factor differential
619 equations, so we are more concerned with the correlation between each other. The
620 correlation must be considered as an important criterion to select the factors, but in

621 order to further verify the correctness of the selection criterion, we have carried out
622 the prediction experiments (the 60 cross-validated retroactive hindcasts experiments
623 of the ENSO index for all seasons combined at lead times of 8 months) of different
624 variables.

625 We can see that for all the forecast results of the models of different variables,
626 the prediction results of T_1, T_2, SOI is the best among those of the three factors and the
627 prediction result of $T_1, T_2, SOI, EAWMI$ is the best among those of the four factors. But
628 the prediction result of $T_1, T_2, SOI, EAWMI$ is best among all, which proves that our
629 selection factors are correct. In our previous study (Hong et al., 2015), the model of
630 the Western Pacific subtropical high was established by using the correlations as a
631 criterion to select factors and their forecast results are also good. Now we use the
632 correlations as a criterion to select factors is also in line with our previous research.

633 The definition of overfitting: The learned hypothesis may fit the training set
634 very well, but fail to predict to new examples (fail to fit additional data or predict
635 future observations reliably).

636 The potential for overfitting depends not only on the number of parameters and
637 data but also the conformability of the model structure with the data shape, and the
638 magnitude of model error compared to the expected level of noise or error in the
639 data(Burnham and Anderson, 2002). So there are many reasons causing the overfitting
640 phenomenon. But this does not mean having many parameters relative to the number
641 of observations inevitably causes the overfitting problem (Golbraikh et al., 2003).
642 There is no evidence that more parameters will be certain to result in overfitting.

643 Based on the definition of overfitting and the previous studies(Golbraikh et al., 2003;
644 Everitt and Skron dal,2010), we can judge whether a model is overfitting or not by the
645 accuracy of prediction results of independent samples (Golbraikh and Tropsha, 2002;
646 Qin and Li, 2006).

647 In the sample training, our model does not purposely pursue the high degree of
648 the training samples fitting and improve the effectiveness of the independent
649 generalization. In fact in our paper the forecast results of the Cross-validated
650 retroactive hindcasts (section 5.2) and the independent samples validation (table3 and
651 table4) are both good. Especially, the independent samples validation of the ENSO
652 index as the table4, we have carried out the 240 independent sample validation
653 prediction of four seasons of different ENSO events and the coverage of independent
654 samples test is very wide. Moreover, compared with 6 mature prediction models, the
655 forecast results of our model are also good, which prove the overfitting problem does
656 not exist in our model. According to the previous literature (Islam and Sivakumar,
657 2002; Sivakumar et al.,2001), we can see that prediction principle and structure of the
658 phase space reconstruction (PSR) of dynamical system is not the same with the
659 traditional neural network and in the small sample situation the forecasting results of
660 PSR model are better than those of the traditional neural network (Sivakumar et
661 al. ,2002), which can be verified in the independent sample test (table3 and table4). So
662 according to the definition of overfitting, we can say the over fitting phenomenon
663 does not exist in our model.

664 Compared with the original model, why the improved model has good forecast

665 results and can overcome the spring predictability barrier to some extent are as follow:
666 Recently, many studies have pointed out that spring is the most unstable season of the
667 air - sea interaction and the error is likely to develop or grow in the spring, resulting in
668 the spring predictability barrier (Zhang et al, 2012; Philander et al., 1992). When the
669 original model uses the indexes in summer as the initial values to predict, the SOI
670 factor representing the air-sea interaction is most unstable in the spring and the
671 EMWMI factor does not have much influence on ENSO in summer, so the forecast
672 results using the indexes in summer as the initial values are certainly much worse than
673 those using the indexes in the winter as the initial values. That is why our original
674 model does not overcome the spring predictability barrier.

675 However, the introduction of the self-memorization dynamics principle can help
676 our model overcome the spring predictability barrier to some extent. Although the
677 lead time is still summer (such as JJA), the information of the initial value actually
678 contains the previous $p + 1$ month (in this case $p = 6$, which contains the information
679 of the previous seven months, including the information of T_1, T_2 , SOI, EMWMI
680 factor in winter (January, February), spring (March, April, May) and summer (June
681 and July)). From the dynamical analysis, in this situation, the information and
682 interaction relationship of four factors have been a long period (from winter to
683 summer) accumulated, containing much air-sea interaction processes and winter
684 monsoon continued abnormal information, so the forecast results of our improved
685 model will be much better than the original model which simply uses only one initial
686 value. That is why the improved model overcomes the spring predictability barrier to

687 some extent.

688 The forecast results of our model are good, but it still has some problems:

689 (1) The inclusion of these terms and the physical processes do these terms in
690 equation (2) represent are important, especially for the discussion of dynamical
691 characteristics of the dynamical model. But now we are difficult to give a clear
692 meaning. Now the main work of our paper is the prediction experiments of the model.
693 For the reason of time and length, this paper mainly discusses the prediction results of
694 the model. The physical processes do these terms represent and the discussion of the
695 dynamical characteristics of the model will be the focus of our next work. Before this,
696 we have also used the Takens' delay embedding theorem to reconstruct the dynamical
697 model of the Western Pacific subtropical high(WPSH). And Based on the
698 reconstructed dynamical model, dynamical characteristics of WPSH are analyzed and
699 an aberrance mechanism is developed, in which the external forcings resulting in the
700 WPSH anomalies are explored, which have been published (Hong et al., 2016). We
701 also study the bifurcation and catastrophe of the West Pacific subtropical high ridge
702 index of a nonlinear model (Hong et al., 2017). Based on our previous method and
703 work, our next work is to analyse the physical processes and the dynamical
704 characteristics of the SST field.

705 (2)The experiments in the present study have proven that the forecasting results
706 of the improved model are good for large-scale systems, such as ENSO events, and
707 the forecasting period has been extended. However, for small-scale systems, such as
708 Hurricanes, whether the forecast results could be improved using the present

709 improved model needs to be further verified.

710 (3) Our paper focuses primarily on these defined indices with T_1, T_2 to
711 reconstruct a prediction model. Maybe, we can select variables (predictor) based on
712 EOF analysis and our model may be a more physically oriented model. Maybe we can
713 learn from Yim et al. (2013; 2015) to draw correlation maps between these fields and
714 the SSTA field and select the predictors from physical considerations. All these above
715 questions require that a lot of experiments to be carried out.

716 These items will be our future work.

717

718 **Acknowledgments** This study was supported by the Chinese National Natural
719 Science Fund (nos 41375002, 41075045, 41306010, 41571017, 51190091 and
720 41071018) and the Chinese National Natural Science Fund (BK20161464) of Jiangsu
721 Province, the Program for New Century Excellent Talents in University
722 (NCET-12-0262), the China Doctoral Program of Higher Education
723 (20120091110026), the Qing Lan Project, the Skeleton Young Teachers Program, and
724 the Excellent Disciplines Leaders in Midlife-Youth Program of Nanjing University.

725

726 **APPENDIX A: THE PRINCIPLE OF DYNAMICAL MODEL**
727 **RECONSTRUCTION**

728 Suppose that the physical law of a nonlinear system going by over time can be
729 expressed as the following difference form:

730
$$\frac{q_i^{(j+1)\Delta t} - q_i^{(j-1)\Delta t}}{2\Delta t} = f_i(q_1^{j\Delta t}, q_2^{j\Delta t}, \dots, q_i^{j\Delta t}, \dots, q_N^{j\Delta t}) \quad j = 2, 3, \dots, M-1 \quad (\text{A1})$$

731 where f_i is the generalized nonlinear function of $q_1, q_2, \dots, q_i, \dots, q_N$, N is the number
732 of variables, and M is the length of observed data. $f_i(q_1^{jM}, q_2^{jM}, \dots, q_i^{jM}, \dots, q_N^{jM})$ can be assumed
733 to contain two parts: G_{jk} representing the expanding items which contain variable
734 q_i , P_{ik} just representing the corresponding parameters which are real numbers
735 ($i = 1, 2, \dots, N, j = 1, 2, \dots, M, k = 1, 2, \dots, K$).

736 It can be supposed as follows:

$$737 \quad f_i(q_1, q_2, \dots, q_n) = \sum_{k=1}^K G_{jk} P_{ik} \quad (\text{A2})$$

738 $D = GP$ is the matrix form of Eq.(A2), in which

$$739 \quad D = \begin{Bmatrix} d_1 \\ d_2 \\ \dots \\ d_M \end{Bmatrix} = \begin{Bmatrix} \frac{q_i^{3\Delta t} - q_i^M}{2\Delta t} \\ \frac{q_i^{4\Delta t} - q_i^{2\Delta t}}{2\Delta t} \\ \dots \\ \frac{q_i^{M\Delta t} - q_i^{(M-2)\Delta t}}{2\Delta t} \end{Bmatrix}, \quad G = \begin{Bmatrix} G_{11}, G_{12}, \dots, G_{1K} \\ G_{21}, G_{22}, \dots, G_{2,K} \\ \dots \\ G_{M1}, G_{M2}, \dots, G_{M,K} \end{Bmatrix}, \quad P = \begin{Bmatrix} P_{i1} \\ P_{i2} \\ \dots \\ P_{iK} \end{Bmatrix} \quad (\text{A3})$$

740 Parameters of the above equation can be determined through inverting the
741 observed data. Vector P which satisfies the above equation can be solved, based on a
742 given vector D. Assuming q is unknown, it is a nonlinear system. However, assuming
743 P is unknown, it is a linear system.

744 With the restriction $S = (D - GP)^T (D - GP)$ as a minimum, GA is introduced as an
745 optimization solution search in the model parameters space.

746 Assuming that the parameters matrix P is the population (solutions), the
747 $S = (D - GP)^T (D - GP)$ is an objective function, $l_i = \frac{1}{S}$ is the value of individual
748 fitness, and $L = \sum_{i=1}^n l_i$ is the value of total fitness. The operating steps of GA include:

749 creation and coding of initial population (solutions), fitness calculation, the choice of
750 male parents, crossover and variation, etc. A detailed theoretical explanation can be

751 got from Wang (2001). The step length is 1 month during the calculation. After
 752 optimization searches and genetic operations, the target value can be rapidly
 753 converged on and each optimal parameter of the dynamical equations can be obtained.

754 Through the above approach, we can obtain parameters of a nonlinear
 755 dynamical system, and reconstruct the nonlinear dynamical equations from observed
 756 data.

757

758 **APPENDIX B: THE MATHEMATICAL PRINCIPLE OF**
 759 **SELF-MEMORIZATION DYNAMICS OF SYSTEMS**

760 The dynamical equations of a system can be expressed as:

761
$$\frac{\partial x_i}{\partial t} = F_i(x, \lambda, t) \quad i = 1, 2, \dots, J \quad (B1)$$

762 where J is an integer, x_i is the i th variable of the system state, and λ is
 763 the parameter. Equation (B1) represents the relationship between a source function
 764 F and a local change of x . Obviously, x is a scalar function with time t and
 765 space r_0 . A set of time $T = [t_{-p} \dots t_0 \dots t_q]$ can be considered, where t_0 is an initial
 766 time. A set of space $R = [r_\alpha \dots r_i \dots r_\beta]$ can be considered, where r_i is a spatial point.

767 An inner product in space $L^2 : T \times R$ is defined by:

768
$$(f, g) = \int_a^b f(\xi)g(\xi)d\xi, f, g \in L^2 \quad (B2)$$

769 Accordingly, a norm can be defined as:

770
$$\|f\| = [\int_a^b (f(\xi))^2 d\xi]^{1/2}$$

771 For a completion L^2 , it can become a Hilbert space H . A generalized one
 772 in H can be regarded as a solution of the multi-time model. By introducing a
 773 memorization function $\beta(r, t)$, we can obtain:

$$774 \quad \int_{t_0}^t \beta(\tau) \frac{\partial x}{\partial \tau} d\tau = \int_{t_0}^t \beta(\tau) F(x, \tau) d\tau \quad (\text{B3})$$

775 where r in $\beta(r, t)$ can be dropped through fixing on the spatial point r_0 . Suppose
 776 that function $\beta(r, t)$ and variable x etc. are all continuous, differentiable and
 777 integrable, an integration by the left parts of Eq. (B3) can be made as:

$$778 \quad \int_{t_0}^t \beta(\tau) \frac{\partial x}{\partial \tau} d\tau = \beta(t)x(t) - \beta(t_0)x(t_0) - \int_{t_0}^t x(\tau)\beta'(\tau)d\tau \quad (\text{B4})$$

779 where $\beta'(t) = \partial\beta(t) / \partial t$. The mean value theorem can be introduced into the third
 780 term in Eq. (B4), the following equation can be obtained:

$$781 \quad -\int_{t_0}^t x(\tau)\beta'(\tau)d\tau = -x^m(t_0)[\beta(t) - \beta(t_0)] \quad (\text{B5})$$

782 where $x^m(t_0) \equiv x(t_m), t_0 < t_m < t$. Substituting Eq. (B4) and Eq. (B5) in Eq. (B3) and
 783 carrying out an algebraic operation, the following equation can be obtained:

$$784 \quad x(t) = \frac{\beta(t_0)}{\beta(t)} x(t_0) + \frac{\beta(t) - \beta(t_0)}{\beta(t)} x^m(t_0) + \frac{1}{\beta(t)} \int_{t_0}^t \beta(\tau) F(x, \tau) d\tau \quad (\text{B6})$$

785 Because the x value which is at initial time t_0 and middle time t_m , only on
 786 the fixed point r_0 itself, relates to the first term and the second term in Eq. (B6),
 787 they are be called as a self-memory term. Also, we can call the third term as an
 788 exogenous effect, i.e., which is contributed by other spatial points.

789 Similarly as Eq. (B4), for multi-time $t_i, i = -p, -p+1, \dots, t_0, t$, it gives

790
$$\int_{t_{-p}}^{t_{-p+1}} \beta(\tau) \frac{\partial x}{\partial \tau} d\tau + \int_{t_{-p+1}}^{t_{-p+2}} \beta(\tau) \frac{\partial x}{\partial \tau} d\tau + \dots + \int_{t_0}^t \beta(\tau) \frac{\partial x}{\partial \tau} d\tau = \int_{t_{-p}}^t \beta(\tau) F(x, \tau) d\tau .$$

791 After the same term $\beta(t_i)x(t_i), i = -p+1, -p+2, \dots, 0$ was eliminated, we

792 have

793
$$\beta(t)x(t) - \beta(t_{-p})x(t_{-p}) - \sum_{i=-p}^0 [\beta(t_{i+1}) - \beta(t_i)]x^m(t_i) - \int_{t_{-p}}^t \beta(\tau)F(x, \tau)d\tau = 0 \quad (\text{B7})$$

794 As a matter of convenience, we set $\beta_t \equiv \beta(t), \beta_0 \equiv \beta(t_0), x_t \equiv x(t), x_0 \equiv x(t_0)$; the

795 following text uses similar notations. Then, Eq. (B7) can be expressed as:

796
$$\beta_t x_t - \beta_{-p} x_{-p} - \sum_{i=-p}^0 x_i^m (\beta_{i+1} - \beta_i) - \int_{t_{-p}}^t \beta(\tau)F(x, \tau)d\tau = 0 \quad (\text{B8})$$

797 Setting $x_{-p} \equiv x_{-p-1}^m, \beta_{-p-1} = 0$, the Eq. (B8) can be written as:

798
$$x_t = \frac{1}{\beta_t} \sum_{i=-p-1}^0 x_i^m (\beta_{i+1} - \beta_i) + \frac{1}{\beta_t} \int_{t_{-p}}^t \beta(\tau)F(x, \tau)d\tau = S_1 + S_2 \quad (\text{B9})$$

799 S_1 is called as a self-memory term and S_2 is called as an exogenous effect term.

800 For the convenience of calculations, the above self-memorization equation can

801 be discretized. The differential by difference and the summation can replace the

802 integration in Eq. (B9), and the mean of two values which are at adjoining times; i.e.,

803
$$x_i^m \approx \frac{1}{2}(x_{i+1} + x_i) \equiv y_i \text{ can simply replace } x_i^m .$$

804 Taking an equal time interval $\Delta t_i = t_{i+1} - t_i = 1$ and incorporating β_i and β_t ,

805 we can obtain a discretized self-memorization equation as follows:

806
$$x_t = \sum_{i=-p-1}^{-1} \alpha_i y_i + \sum_{i=-p}^0 \theta_i F(x, i) \quad (\text{B10})$$

807 where F is the dynamic kernel of the self-memorization equation, $\alpha_i = \frac{(\beta_{i+1} - \beta_i)}{\beta_t}$;

808
$$\theta_i = \frac{\beta_i}{\beta_t} .$$

809 Based on Eq. (B10), the above technique performed computations and the
810 forecast can be called as a self-memorization principle.

811

812

813 REFERENCES

814 Ashok K, Guan Z, Yamagata T : Impact of the Indian Ocean Dipole on the decadal relationship
815 between the Indian monsoon rainfall and ENSO, *Geophys Res Lett*,28(23), 4499-4502, 2001.

816 Balmaseda M.A., Davey M.K. and Anderson D.L.T.: Decadal and seasonal dependence of ENSO
817 prediction skill,*J Clim.*,8, 2705–2715, 1995.

818 Barnston A. G., et al.: Skill of real-time seasonal ENSO model predictions during 2002-2011,*Bull.*
819 *Amer. Meteor. Soc.*,93, 631-651, 2012.

820 Belkin M. and P. Niyogi: Laplacian eigenmaps for dimensionality reduction and data
821 representation,*Natural Comput.*,15,1373-1391, 2003.

822 Bjerknes J.: Atmospheric teleconnections from the equatorial Pacific,*Mon. Wea. Rev.*,97,163-172, 1969.

823 Burnham, K. P.; Anderson, D. R: *Model Selection and Multimodel Inference* (2nd ed.),
824 Springer-Verlag, 2002.

825 Cao H. X.: Self-memorization Equation in Atmospheric Motion,*Science in China (Series B)*,36(7),
826 845-855, 1993.

827 Chen D., S. E. Zebiak, A. J. Busalacchi and M. A. Cane: An Improved Procedure for El Niño
828 Forecasting: Implications for Predictability,*Science*, 269, 1699-1702, 1995.

829 Chen G., Shao B. M. Han Y., et al.: Modality of semiannual to multidecadal oscillations in global sea
830 surface temperature variability. *Journal of Geophysical Research*, 115, 1-14, 2010.

831 Chen X. D., Xia J., Xu Q.: Differential Hydrological Grey Model(DHGM) with self-memory function
832 and its application to flood forecasting,*Sci China Tech Sci.*,52,1039–1049, 2009.

833 Clarke A. J. and S. Van Gorder: Improving El Niño prediction using a space-time integration of
834 Indo-Pacific winds and equatorial Pacific upper ocean heat content, *Geophys. Res. Lett.*,30,1399.
835 doi:10.1029/2002GL016673, 2003.

836 Delecluse P., Davey M., Kitamura Y., Philander S., Suarez M., Bengtsson L.: TOGA review paper:
837 coupled general circulation modeling of the tropical Pacific,*J Geophys Res*,103,14357–14373, 1998.

838 Davey M., Huddleston M., Sperber K.R., et al.: A study of coupled model climatology and variability
839 in tropical ocean regions, *Clim. Dyn.*, 18, 403–420, 2002.

840 Dommenges and Latif: A Cautionary Note on the Interpretation of EOFs, *Journal of*
841 *Climate*, 15(2), 216–225, 2002.

842 Drosowsky W.: Statistical prediction of ENSO (Niño 3) using sub-surface temperature data, *Geophys.*
843 *Res. Lett.*, 33, L03710. doi:10.1029/2005GL024866, 2006.

844 Everitt B.S., Skrondal A.: *Cambridge Dictionary of Statistics*, Cambridge University Press, 2010.

845 Feng G. L., Cao H. X., Gao X. Q., et al.: Prediction of precipitation during summer monsoon with
846 self-memorial model, *Adv Atmos Sci.*, 18, 701–709, 2001.

847 Fraedrich K.: Estimating weather and climate predictability on attractors, *J. Atmos. Sci.*, 44, 722–728,
848 1987.

849 Glantz MH, Katz RW, Nicholls N (eds): *Teleconnections linking worldwide climate anomalies*,
850 74pp, Cambridge University Press, Cambridge, UK, 1991.

851 Golbraikh A. and Tropsha A.: Beware of q^2 ! *Journal of Molecular Graphics and Modelling*, 20 ,
852 269–276, 2002.

853 Golbraikh A., Shen M., Xiao Z. Y., Xiao Y. D., Lee Kuo-Hsiung, Tropsha A.: Rational selection of
854 training and test sets for the development of validated QSAR models. *Journal of Computer-Aided*
855 *Molecular Design*, 17(2), 241–253, 2003.

856 Gu X. Q.: A spectral model based on atmospheric self-memorization principle, *Chinese Science*
857 *Bulletin*, 43(20), 1692–1702, 1998.

858 Hong M., Zhang R., Wu G. X., et al.: A Nonlinear Dynamic System Reconstruction of the Subtropical
859 High Characteristic Index based on Genetic Algorithm. *Chinese Journal of Atmospheric*
860 *Sciences*, 31(2):346–352, 2007.

861 Hong M., Zhang R. and Ma C. C. et al.: A Non-Linear Dynamical–Statistical Model for Reconstruction
862 of the Air–Sea Element Fields in the Tropical Pacific Ocean, *Atmosphere–Ocean*, doi:
863 10.1080/07055900.2014.908765, 2014.

864 Hong M., Zhang R., et al.: Reconstruction and forecast experiments of a statistical-dynamical model of
865 the Western Pacific subtropical high and Eastern Asian summer monsoon factors, *Weather and*
866 *Forecasting*, 30:206–216, 2015

867 Hong M., Zhang R., et al.: Catastrophe and Mechanism Analyses of Multiple Equilibria in the Western

868 Pacific Subtropical High System Based on Objective Fitting of Spatial Basis Functions. *Monthly*
869 *Weather Review*, 144, 997-1015, 2016.

870 Hong M., Zhang R., et al.: Bifurcations and catastrophes in a nonlinear dynamical model of the western
871 Pacific subtropical high ridge line index and its evolution mechanism, *Theor. Appl. Climatol.*, 129,
872 363-384, 2017.

873 Hu, T.S., K.C. Lam, and S.T. Ng: River flow time series prediction with a range-dependent neural
874 network, *Hydrol. Sci. J.*, 46, 729–745, 2001.

875 Hu Y. J., Zhong Z., Zhu Y. M. et al.: A statistical forecast model using the time-scale decomposition
876 technique to predict rainfall during flood period over the middle and lower reaches of the Yangtze
877 River Valley. *Theoretical and Applied Climatology*, doi: 10.1007/s00704-017-2094-9, 2017.

878 Huang. J., Y. Yi, S. Wang, et al.: An analogue-dynamical long-range numerical weather prediction
879 system incorporating historical evolution, *Quart J Roy Meteor Soc*, 119(511), 547-565, 1993.

880 Islam M.N. Sivakumar B.: Characterization and prediction of runoff dynamics: a nonlinear dynamical
881 view. *Advances in Water Resources*, 25, 179-190, 2002.

882 James A. Carton and Benjamin S. Giese: A Reanalysis of Ocean Climate Using Simple Ocean Data
883 Assimilation (SODA), *Monthly Weather Review*, 136(8), 2999-3011, 2008.

884 Jin E. K., James L. K., Wang B., et al.: Current status of ENSO prediction skill in coupled
885 ocean-atmosphere models, *Climate Dyn*, 31, 647-664, 2008.

886 Johnson S.D., Battistis D.S. and Sarachik E. S.: Empirically Derived Markov Models and Prediction of
887 Tropical Pacific Sea Surface Temperature Anomalies, *Journal of Climate*, 13, 3-17, 2000.

888 Kalnay E., Kanamitsu M. and Kistler R.: The NCEP/NCAR 40-year reanalysis project, *Bull. Amer.*
889 *Meteor. Soc.*, 77, 437-470, 1996.

890 Kathrin Büttner, Jennifer Salau, and Joachim Krieter: Temporal correlation coefficient for directed
891 networks. *Springerplus*, 5(1): 1198-1203, 2016.

892 Kim Ji-Won, Soon-Il An, Sang-Yoon Jun, Hey-Jin Park, Sang-Wook Yeh.: ENSO and East Asian winter
893 monsoon relationship modulation associated with the anomalous northwest Pacific anticyclone,
894 *Climate Dynamics*, 49(4), 1157–1179, 2017.

895 L'Heureux Michelle L., Collins Dan C., Hu Zeng-Zhen. Linear trends in sea surface temperature of the
896 tropical Pacific Ocean and implications for the El Niño-Southern Oscillation, *Climate Dynamics*, 40,
897 1223–1236, 2013.

898 Liebmann B. and C.A. Smith: Description of a Complete (Interpolated) Outgoing Longwave Radiation

899 Dataset, *Bulletin of the American Meteorological Society*, 77, 1275-1277, 1996.

900 Luo, J.-J., S. Masson, S. Behera, S. Shingu, and T. Yamagata: Seasonal climate predictability in a
901 coupled OAGCM using a different approach for ensemble forecasts, *J. Climate*, 18, 4474–4497, 2005.

902 Mechoso C.R., Robertson A.W., Barth N., et al.: The seasonal cycle over the tropical Pacific in coupled
903 atmosphere–ocean general circulation models, *Mon Weather Rev*, 123, 2825–2838, 1995.

904 Molteni F., et al.: ECMWF seasonal forecast system 3, *CLIVAR Exch*, 43, 7-9, 2007.

905 Moore A. M., Zavala-Garay J. and Tang Y., et al.: Optimal forcing patterns for coupled models of
906 ENSO, *J Climate*, 19, 4683-4699, 2006.

907 Neelin J.D., Latif M. and Allaart M.A.F.: Tropical air-sea interaction in general circulation
908 models, *Clim Dyn.*, 7, 73–104, 1992.

909 Nicosia V, Tang J, Mascolo C, Musolesi M, Russo G, Latora V: Graph metrics for temporal networks.
910 In: Holme P, Saramäki J, editors. *Temporal networks*. Berlin: Springer, pp. 15–40, 2013,.

911 Palmer T. N., Alessandri A. and Andersen U., et al.: Development of a European multi-model
912 ensemble system for seasonal to interannual prediction (DEMETER), *Bull Amer Met Soc.*, 85, 853-872 ,
913 2004.

914 Philander S G, Pacanowski R.C., N-C Lau et al.: Simulation of ENSO with a global atmospheric GCM
915 coupled to a high resolution, tropical Pacific Ocean GCM. *J. Climate*, 5, 308-329, 1992.

916 Qin G. H. and Li Z. H.: Over-fitting of BP NN research and its application, *Engineering Journal of*
917 *Wuhan University*, 39(6), 1671-1679, 2006.

918 Rasmusson E.M. and Carpenter T.H.: Variations in tropical sea surface temperature and surface wind
919 fields associated with the Southern Oscillation/El Niño, *Mon Weather Rev.*, 10, 354-384, 1982.

920 Rayner NA, Parker DE, Horton EB, Folland CK, Alexander LV, Rowell DP, Kent EC, Kaplan A:
921 Global analyses of sea surface temperature, sea ice, and night marine air temperature since the late
922 nineteenth century. *J Geophys Res* 108(D14):4407. doi:10.1029/2002JD002670, 2003.

923 Reynolds, R. W., N. A. Rayner, T. M. Smith, D. C. Stokes, and W. Wang: An improved in situ and
924 satellite SST analysis for climate, *J. Climate*, 15, 1609–1625, 2002.

925 Saha S., Nadiga C. and Thiaw J., et al.: The NCEP climate forecast system, *Journal of*
926 *Climate*, 19, 3483-3517, 2006.

927 Saji N. H., Goswami B. N., Vinayachandran P. N., et al.: A dipole mode in the tropical Indian

928 Ocean,Nature, 401(6751),360-363, 1999.

929 Smith T.M.: Improved extended reconstruction of SST(1854-1997). J. Climate, 17, 2466-2477, 2004.

930 Takens, F.: Detecting strange attractors in fluid turbulence,Lecture Notes in
 931 Mathematics,898(2),361-381 , 1981.

932 Sivakumar B, Berndtsson R, Persson M.: Monthly Runoff Prediction Using Phase -space
 933 Reconstruction. Hydrological Sciences Journal, 46(3), 377 -388, 2001.

934 Sivakumar B., Jayawardena A.W., Fernando T.M.K.G.,: River flow forecasting: use of phase-space
 935 reconstruction and artificial neural networks approaches. Journal of Hydrology, 265, 225-245, 2002.

936 Timmermann A., Voss H. U. and Pasmanter R.: Empirical Dynamical System Modeling of ENSO
 937 Using Nonlinear Inverse Techniques, Journal of Physical Oceanography, 31,1579-1598 , 2001.

938 Tomita, T., and T. Yasunari: Role of the northeast winter monsoon on the biennial oscillation of the
 939 ENSO/monsoon system,J. Meteor. Soc. Japan, 74,399–413 , 1996.

940 Trenberth, E. K., et al.: Progress during TOGA in understanding and modeling global teleconnections
 941 associated with tropical sea surface temperatures,J. Geophys. Res., 107, C7, 14291-14324,1998.

942 Wang B., Wu R., Lukas R.: Roles of western North Pacific wind variation in thermocline adjustment
 943 and ENSO phase transition,J Meteor Soc Japan,77,1-16,1999a.

944 Wang B., Wu R., Li T.: Atmosphere-warm ocean interaction and its impacts on Asian-Australian
 945 monsoon variation. J. Climate, 16, 1195-1211, 2003.

946 Wang B., Lee J. Y., Shukla J., et al.: Advance and prospectus of seasonal prediction: assessment of
 947 the APCC / CliPAS 14-Model Ensemble Retrospective Seasonal Prediction(1980—2004),Climate
 948 Dyn.,33(1),93-117 , 2009a.

949 Wang C., Weisberg R. H. and Virmani J. I.: Western Pacific interannual variability associated with the
 950 El Niño-Southern Oscillation,J Geophy Res.,104,5131-5149, 1999b.

951 Wang, L., W. Chen, and R. H. Huang: Interdecadal modulation of PDO on the impact of ENSO on the
 952 east Asian winter monsoon, Geophys. Res. Lett., 35, L20702, doi:10.1029/2008GL035287, 2008.

953 Wang, W. C., K. W. Chau, C. T. Cheng, and L. Qiu: A comparison of performance of several artificial
 954 intelligence methods for forecasting monthly discharge time series. J. Hydrol., 374, 294–306,
 955 doi:10.1016/j.jhydrol.2009.06.019,2009b.

956 Wang L.: Intelligent Optimization Algorithms and Its Application, pp. 23-24, Tsinghua University
 957 Press, Chendu, 2001.

958 Webster P. J., Moore A. M., Loschnigg J. P., et al.: Coupled ocean-atmosphere dynamics in the Indian
959 Ocean during 1997- 98, *Nature*, 401(6751),356-360, 1999.

960 Weinberger K. Q. and L. Saul: Unsupervised learning of image manifolds by semidefinite
961 programming, *Int. J. Comput. Vision.*,70, 77-90, 2006.

962 Xu B.C., Wang Z.S., Wu J.P. and Zhou E.M.: Interaction between sea surface temperature (SST) of
963 information regions and southern oscillation index (SOI) in Tropical Pacific Ocean. *Marine Science*
964 *Bulletin*, 12(5),211-25,1993.

965 Yang, S., K. M. Lau, and K. M. Kim: Variations of the East Asian jet stream and
966 Asian-Pacific-American winter climate anomalies, *J. Climate*, 15,306–325 , 2002.

967 Yang Se-Hwan and Lu Riyu: Predictability of the East Asian winter monsoon indices by the coupled
968 models of ENSEMBLES, *Advances in Atmospheric Sciences*, 31(6), 1279–1292, 2014

969 Yim SY, Wang B, Kwon M: Interdecadal change of the controlling mechanisms for East Asian early
970 summer rainfall variation around the mid-1990s. *ClimDyn.*, 42,1325–1333, 2013.

971 Yim, S.-Y., B. Wang, W. Xing, M.-M.Lu: Prediction of Meiyu rainfall in Taiwan by multi-lead
972 physicalempiricalmodels. *Clim. Dyn.*, 44 (11-12), 3033-3042, doi:10.1007/s00382-014-2340-0, 2015.

973 Yoon, J., and S. W. Yeh: Influence of the Pacific Decadal Oscillation on the relationship between El
974 Niño and the northeast Asian summer monsoon, *J. Climate*,23, 4525–4537, 2010.

975 Yu H., J. Huang, and J. Chou: Improvement of Medium-Range Forecasts Using the
976 Analogue-Dynamical Method, *Mon. Wea. Rev.*, 142, 1570–1587, doi:
977 <http://dx.doi.org/10.1175/MWR-D-13-00250.1>, 2014a.

978 Yu H., J. Huang, W. Li, and G. Feng: Development of the analogue-dynamical method for error
979 correction of numerical forecasts, *J. Meteor. Res.*, 28(5), 934–947, doi: 10.1007/s13351-014-4077-4 ,
980 2014b.

981 Zhang R. and Hong M., et al.: Non-linear Dynamic Model Retrieval of Subtropical High Based on
982 Empirical Orthogonal Function and Genetic Algorithm, *Applied Mathematics and*
983 *Mechanics*,27(12),1645-1654, 2006.

984 Zhang R. and Hong M.,et al.: Retrieval of the non-linear dynamic forecast model of El Nino/La Nina
985 index based on the genetic algorithm optimization. *Chinese Journal of Geophysics*,51(5),1354-1362,
986 2008.

987 Zhang R. H., Zhou G. Q. and Chao J. P.: ENSO Dynamics and Its Prediction, *Chinese Journal of*

988 Atmospheric Sciences,27(4) ,674-688, 2003a.

989 Zhang, R.H., S. E. Zebiak, R. Kleeman, and N.Keenlyside: A new intermediate coupled model for El
990 Niño simulation and prediction. Geophys. Res.Lett., 30, doi:10.1029/2003GL018010, 2003b.

991 Zhang, R. H., A. Sumi, and M. Kimoto: Impact of El Niño on the East Asian monsoon: A diagnostic
992 study of the '86/87 and '91/92 events,J. Meteor. Soc. Japan, 74, 49–62, 1996.

993 Zhang Y. L., Yu Y. Q., Duan W. S.: The spring prediction barrier of ENSO in retrospective prediction
994 experiments as shown by the four coupled ocean-atmosphere models. Acta Meteorologica Sinica, 70(3),
995 506-519, 2012.

996 Zhao J. H., Liu X. Y. and Jiang H. Y., et al.: Characteristics of Sea Surface Height in Tropical Pacific
997 and its relationship with ENSO events,Meteorological and Environmental Sciences, 35(2),33-39, 2012.

998 Zhou, L.-T., and R. G. Wu: Respective impacts of the East Asian winter monsoon and ENSO on winter
999 rainfall in China,J. Geophys. Res.,115, doi: 10.1029/2009JD012502, 2010.

1000
1001
1002
1003
1004
1005
1006
1007
1008
1009
1010
1011
1012
1013
1014
1015
1016
1017
1018
1019
1020
1021
1022
1023
1024
1025

1026 **List of Figures:**

1027 **Fig.1**(a, c) First and second modes of the EOF deconstruction of the SSTA field, and (b, d) the
1028 corresponding PC time series.

1029 **Fig. 2** Forecast results of the first time coefficient series (a) and the second time coefficient series (b) of
1030 the SSTA field by the original model

1031 **Fig. 3.** The cross-validated retroactive hindcast results of the first time coefficient series (a) and the
1032 second time coefficient series (b) of the SSTA field by the original model

1033 **Fig. 4.** Long-term step-by-step forecast results of the first time coefficient series (a) and the second
1034 time coefficient series (b) of the SSTA field by the improved model

1035 **Fig. 5.** The cross-validated retroactive hindcast results of the first time coefficient series (a) and the
1036 second time coefficient series (b) of the SSTA field by the improved model

1037 **Fig. 6.** The forecast SSTA field (a) and the actual SSTA field (b) of an El Niño event (Dec.1997)

1038 **Fig. 7.** The forecast SSTA field (a) and the actual SSTA field (b) of a La Niña event (Dec.1999)

1039 **Fig. 8.** The forecast SSTA field (a) and the actual SSTA field (b) of neutral event (Nov.2002)

1040 **Fig. 9.** The improved dynamical-statistical model prediction of the ENSO index

1041 **Fig. 10.** Temporal correlation between model forecasts and observations for all seasons combined, as a
1042 function of lead time. Each line highlights one model.

1043 **Fig.11.** RMSE in standardized units, as a function of lead time for all seasons combined. Each line
1044 highlights one model.

1045

1046

1047

1048

1049

1050 **Table captions:**

1051 **Table 1.** The correlation analysis between the front two time series T_1, T_2 and nine impact factors

1052 **Table2.** The CC and MAPE of long-term fitting test when the retrospective order p is different

1053 **Table3.** The forecast results of T_1 and T_2 in different examples within 6 and 12 months

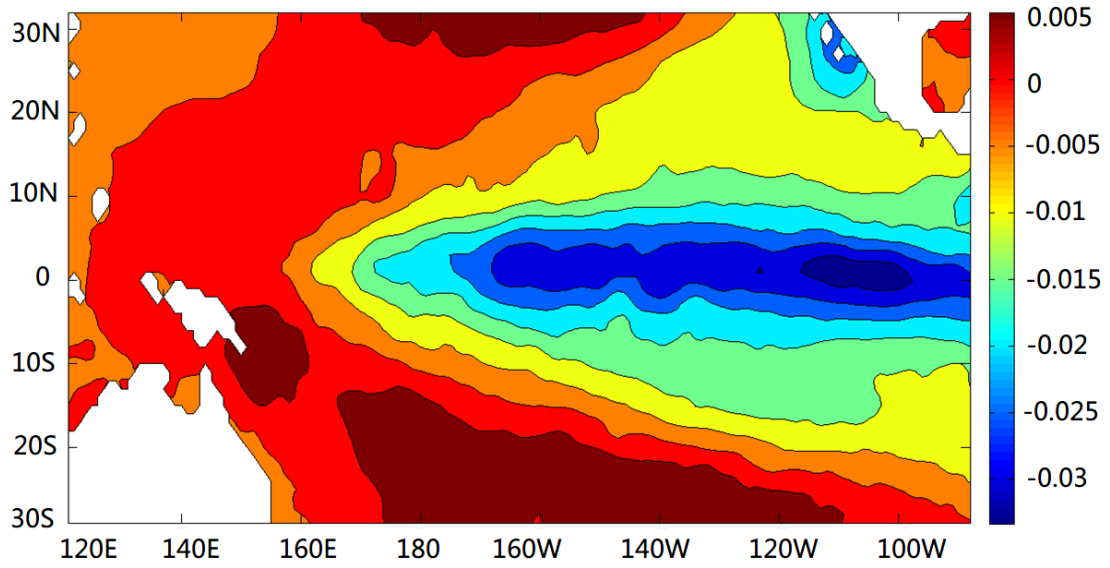
1054 **Table. 4.** The TC and the MAPE between model forecasts and observations within 12 months for
1055 Nov.–Jan., Dec.–Feb., and Jan.–Mar. as lead time of winter, for Feb.–Apr. , Mar.–May and Apr.–June as
1056 lead time of spring, for May-July, June-August and July-Sep. as lead time of summer and for
1057 August-Oct., Sep.-Nov. and Oct.-Dec. as lead time of autumn.

1058 **Table5.** The forecast results of the different data periods

1059

1060

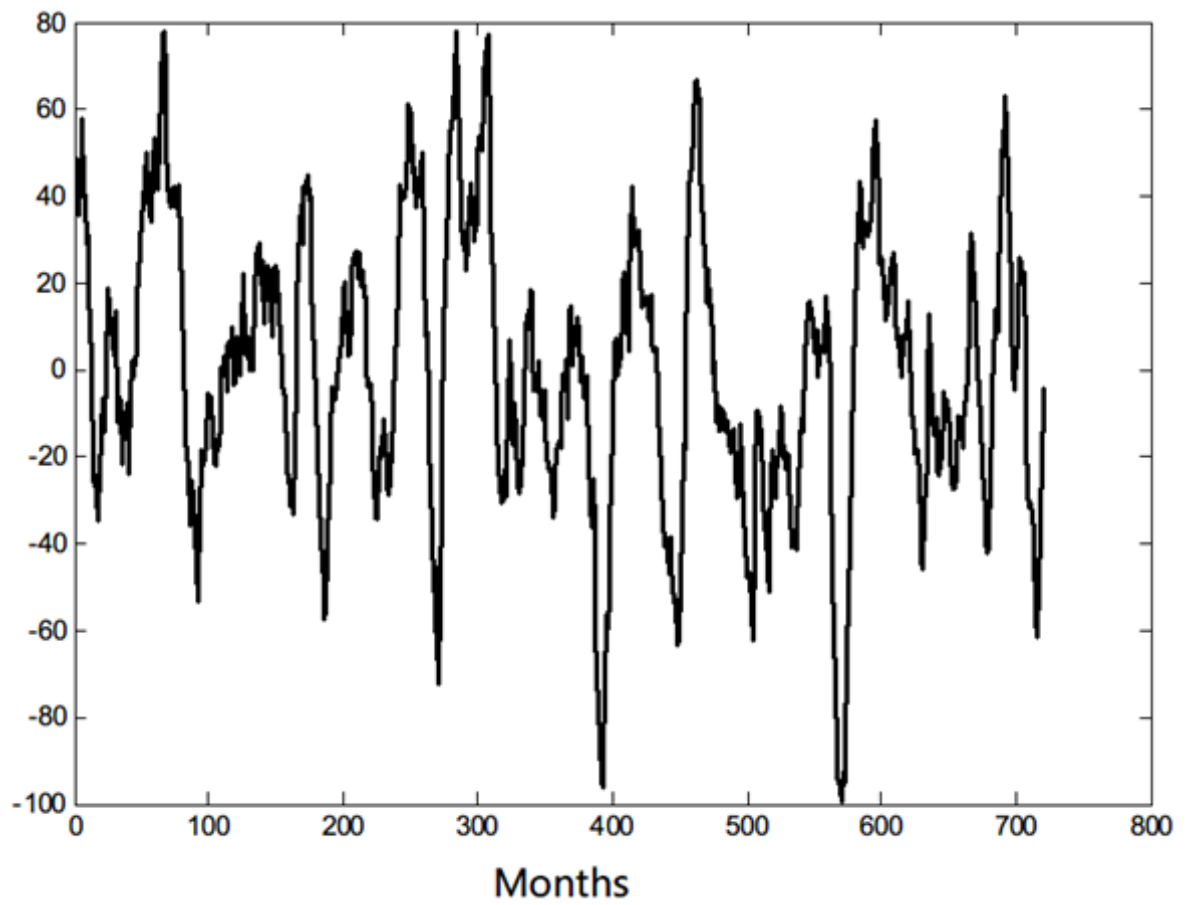
1061 **Figure:**



1062

1063

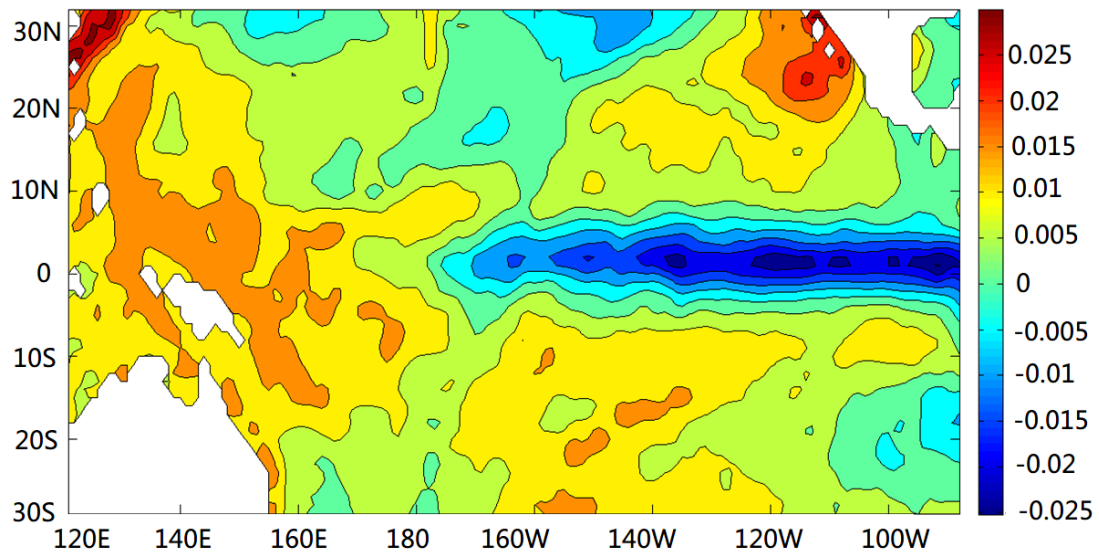
(a)



1064

1065

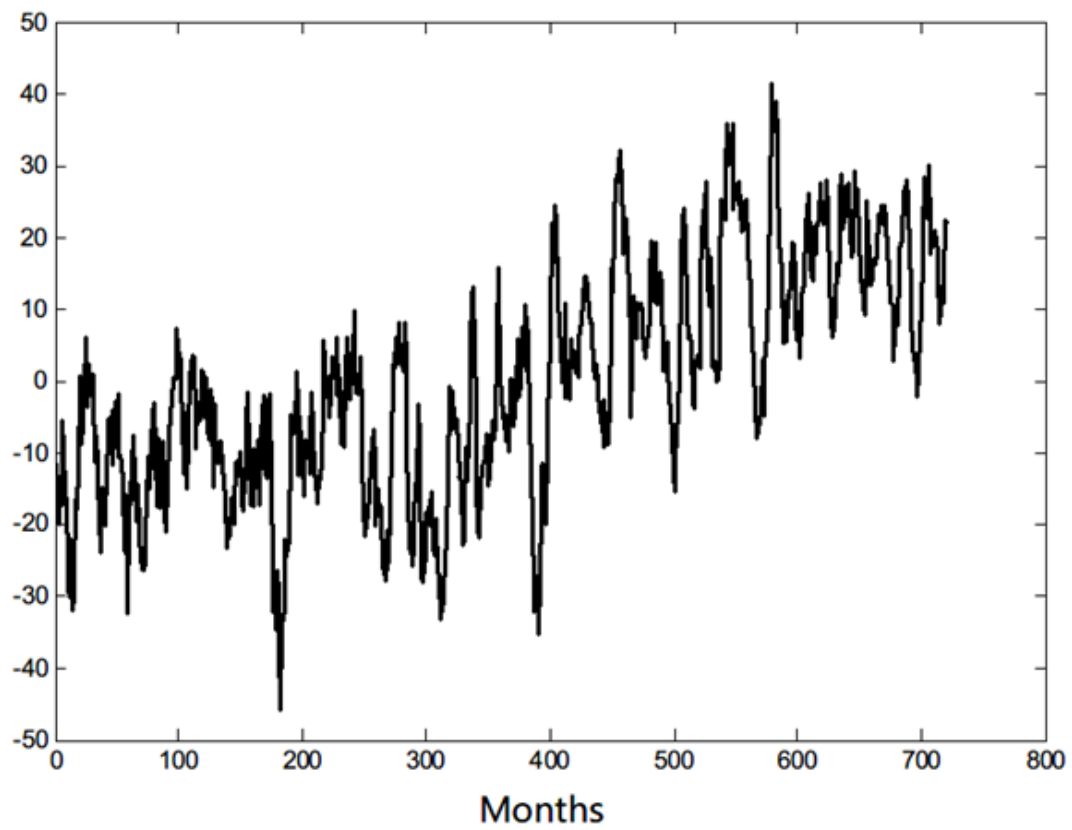
(b)



1066

1067

(c)



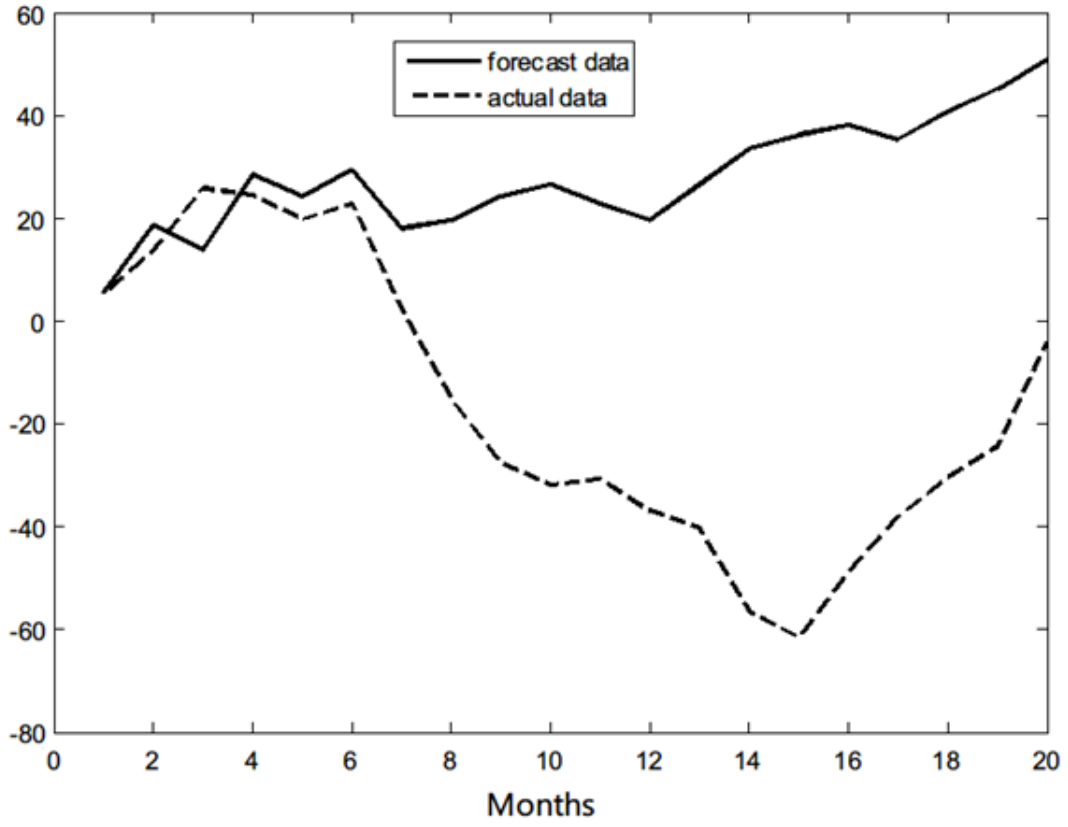
1068

1069

(d)

1070 **Fig. 1** (a, c) First and second modes of the EOF deconstruction of the SSTA field, and (b, d) the

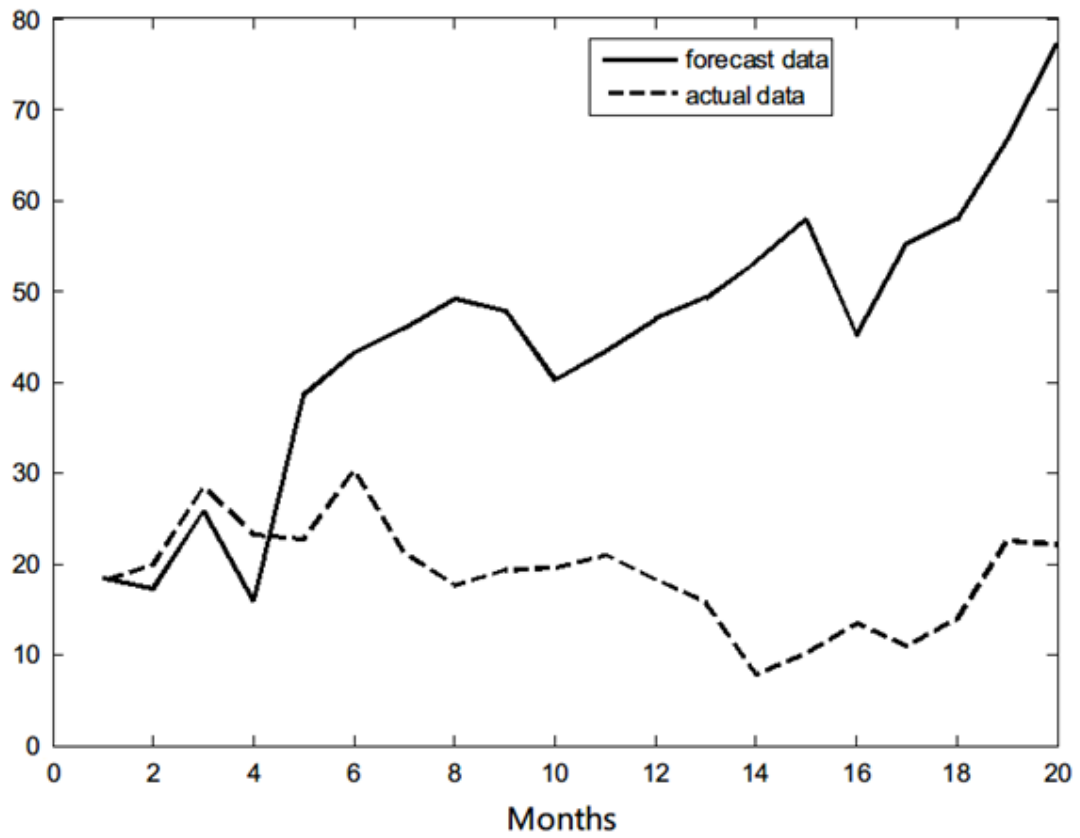
1071 corresponding PC time series.



1072

1073

(a)



1074

1075

(b)

1076 Fig.2 Forecast results of the first time coefficient series T_1 (a) and the second time coefficient series

1077 T_2 (b)of the SSTA field by the original model

1078

1079

1080

1081

1082

1083

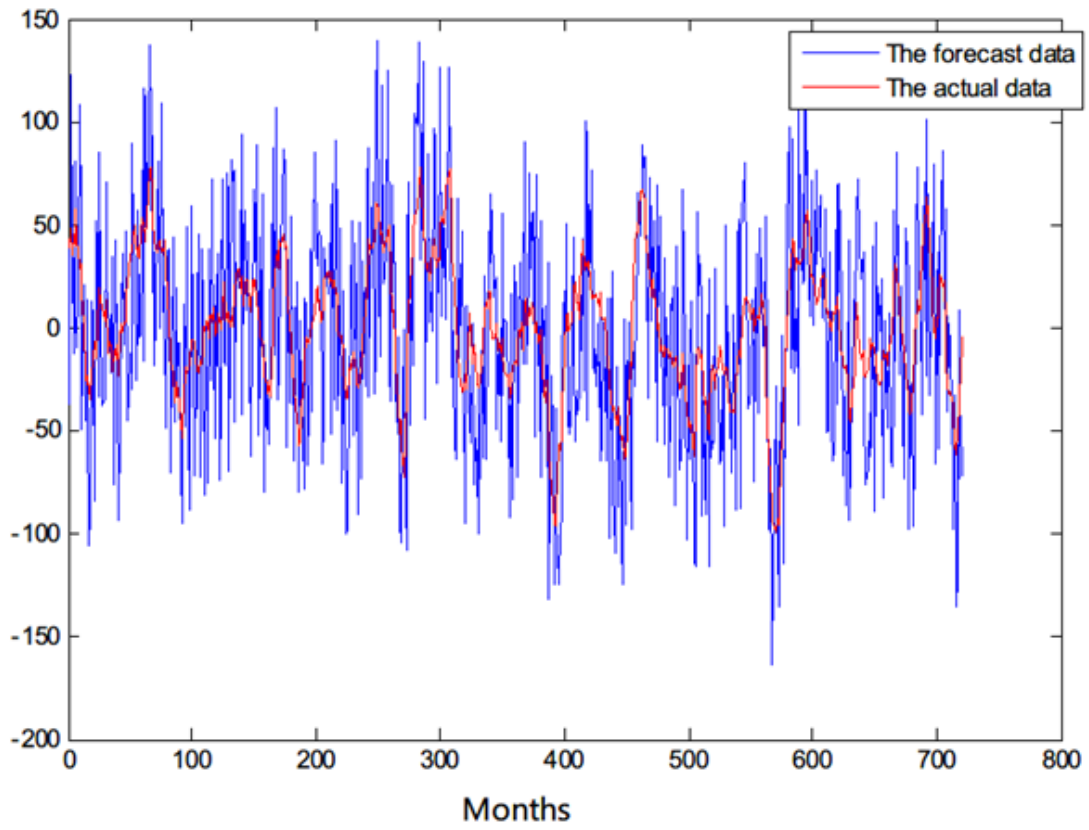
1084

1085

1086

1087

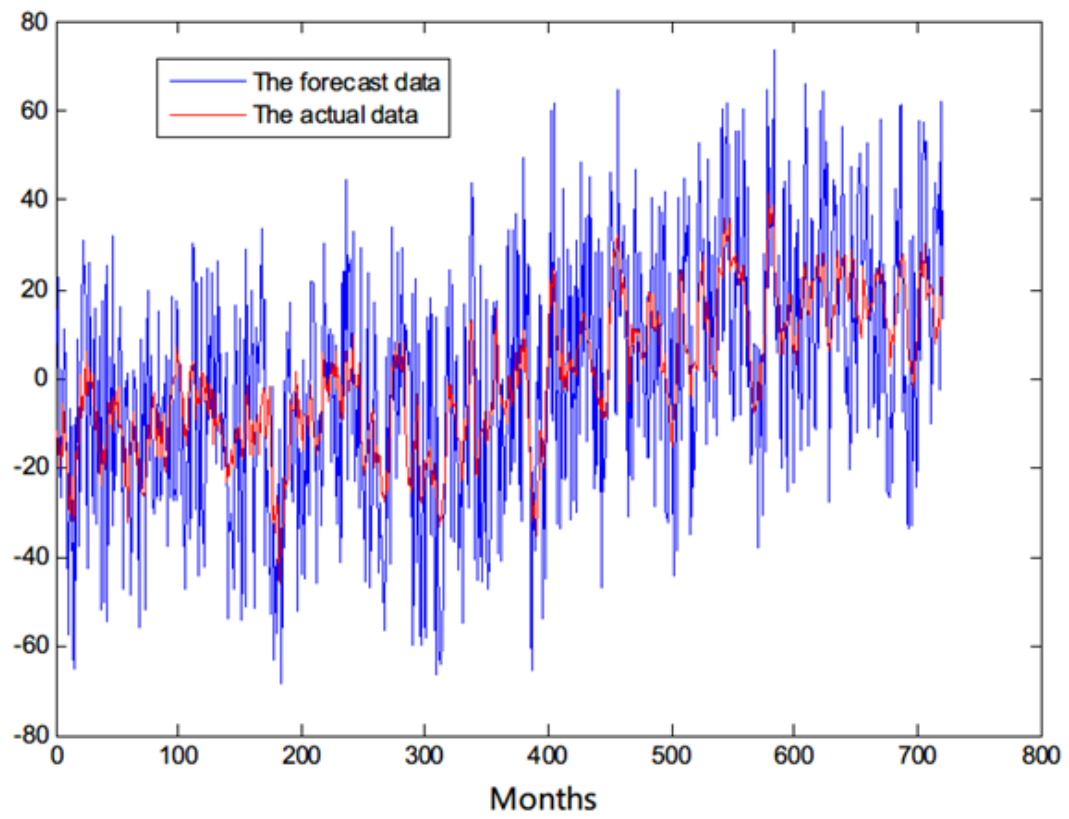
1088



1089

1090

(a)



1091

1092

(b)

1093 Fig.3The cross-validated retroactive hindcast results of the first time coefficient series T_1 (a)and the
1094 second time coefficient series T_2 (b)of the SSTA field by the original model

1095

1096

1097

1098

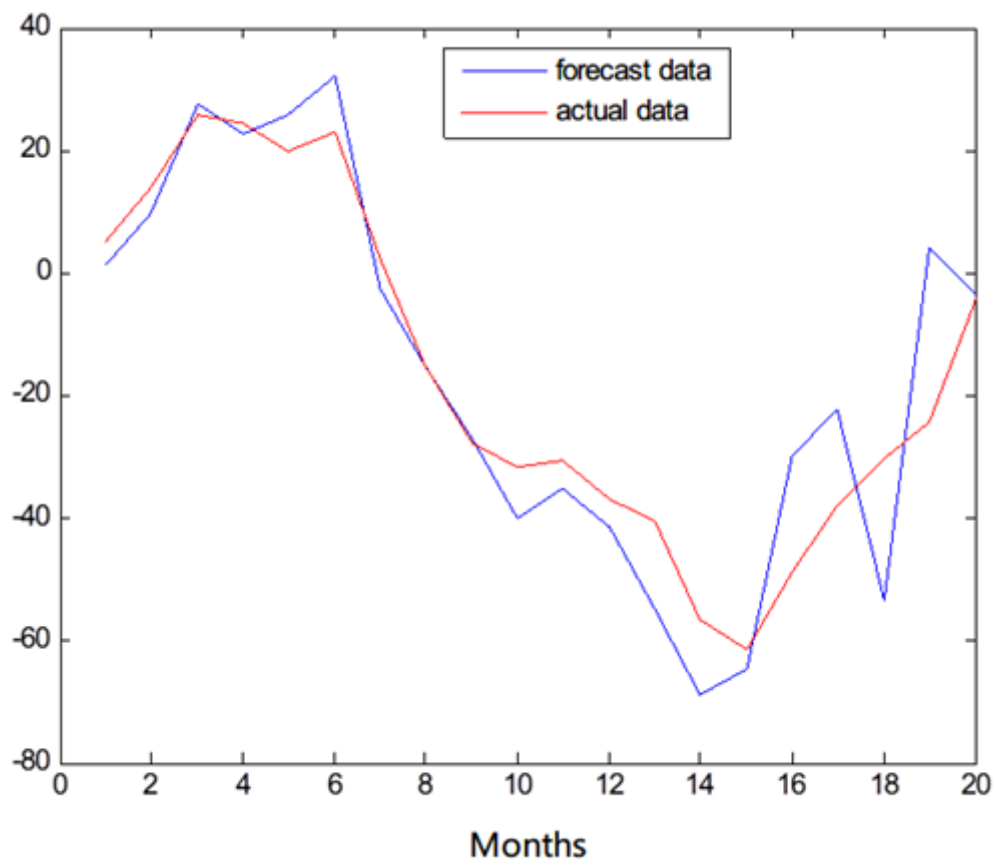
1099

1100

1101

1102

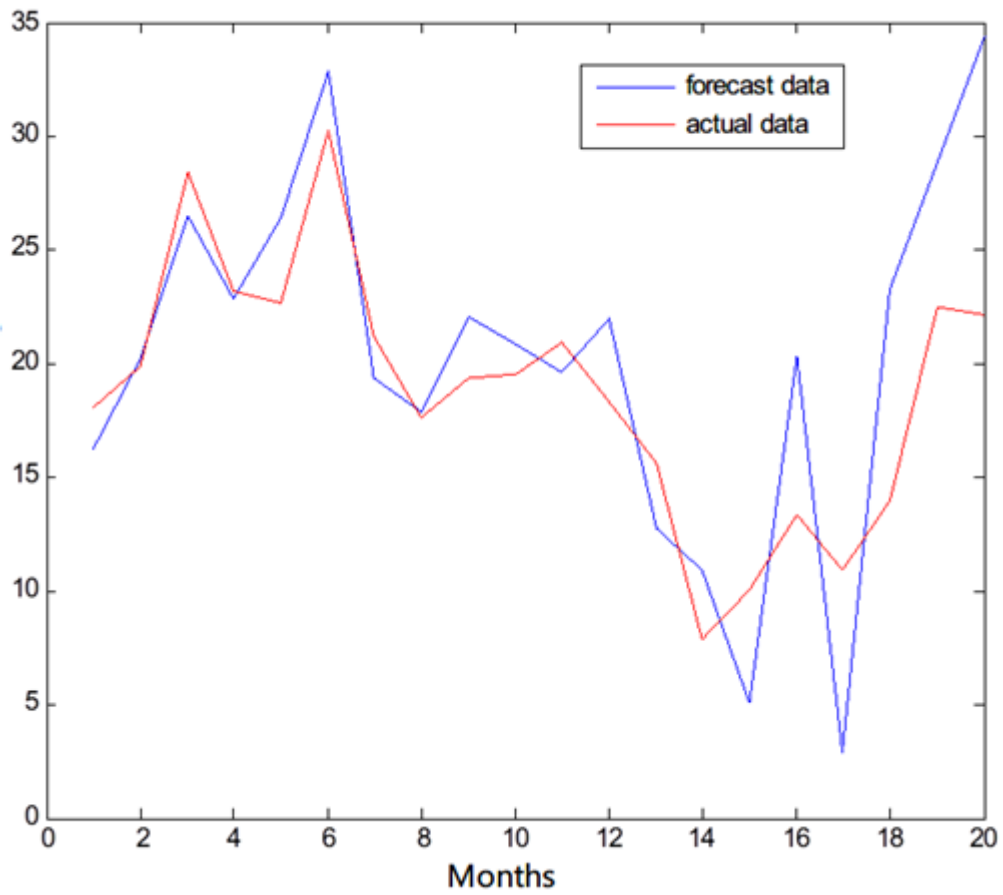
1103



1104

1105

(a)



1106

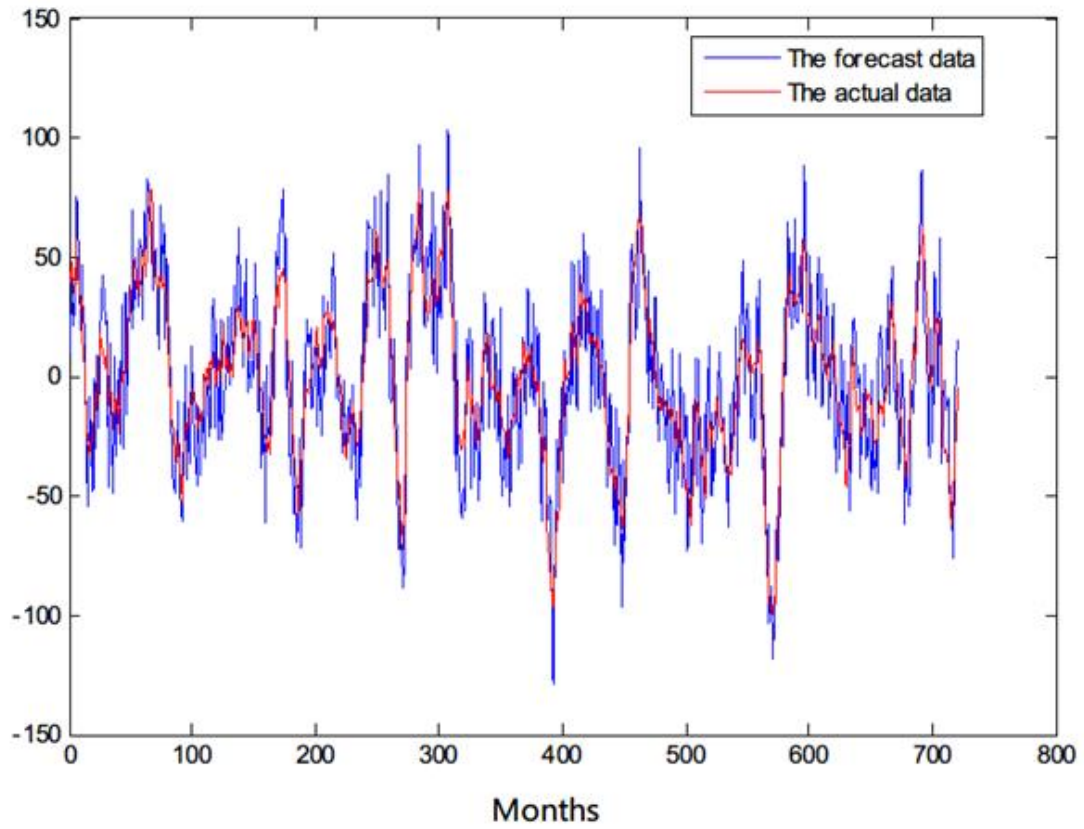
1107

(b)

1108 Fig. 4. Long-term step-by-step forecast results of the first time coefficient series T_1 (a) and the second

1109 time coefficient series T_2 (b) of the SSTA field by the improved model

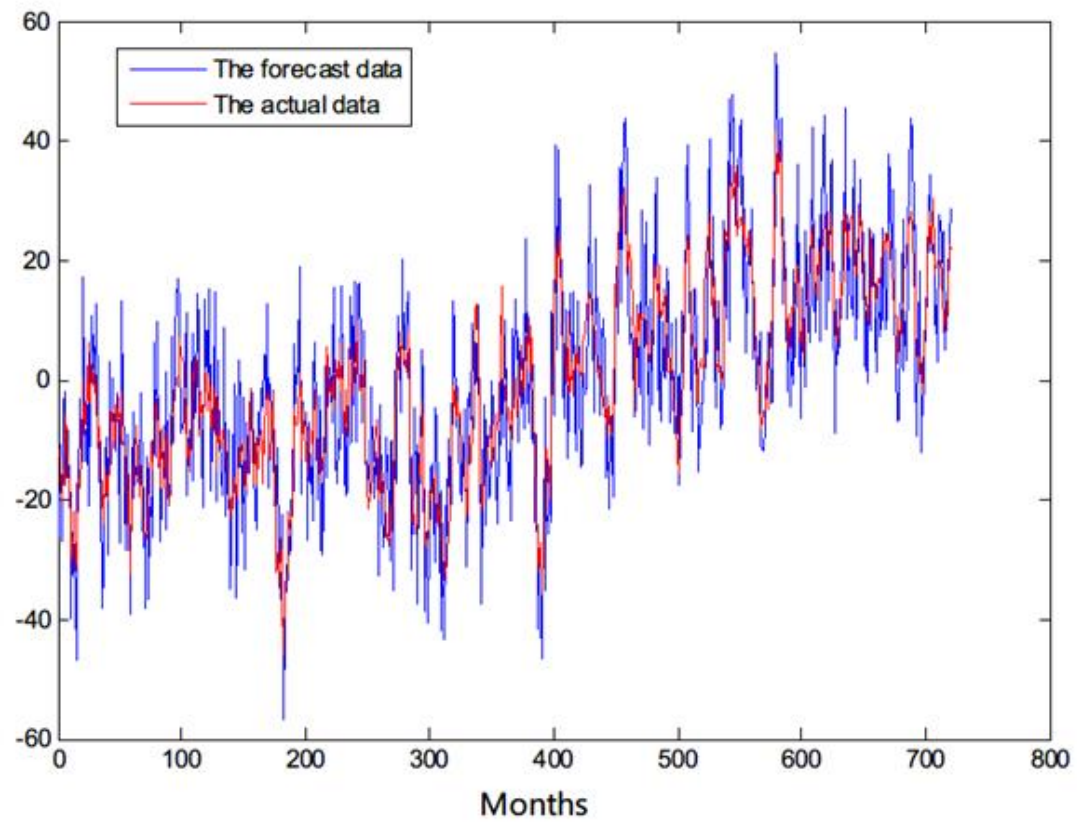
1110



1111

1112

(a)



1113

1114

(b)

1115 Fig. 5. The cross-validated retroactive hindcast results of the first time coefficient series T_1 (a) and the
1116 second time coefficient series T_2 (b) of the SSTA field by the improved model

1117

1118

1119

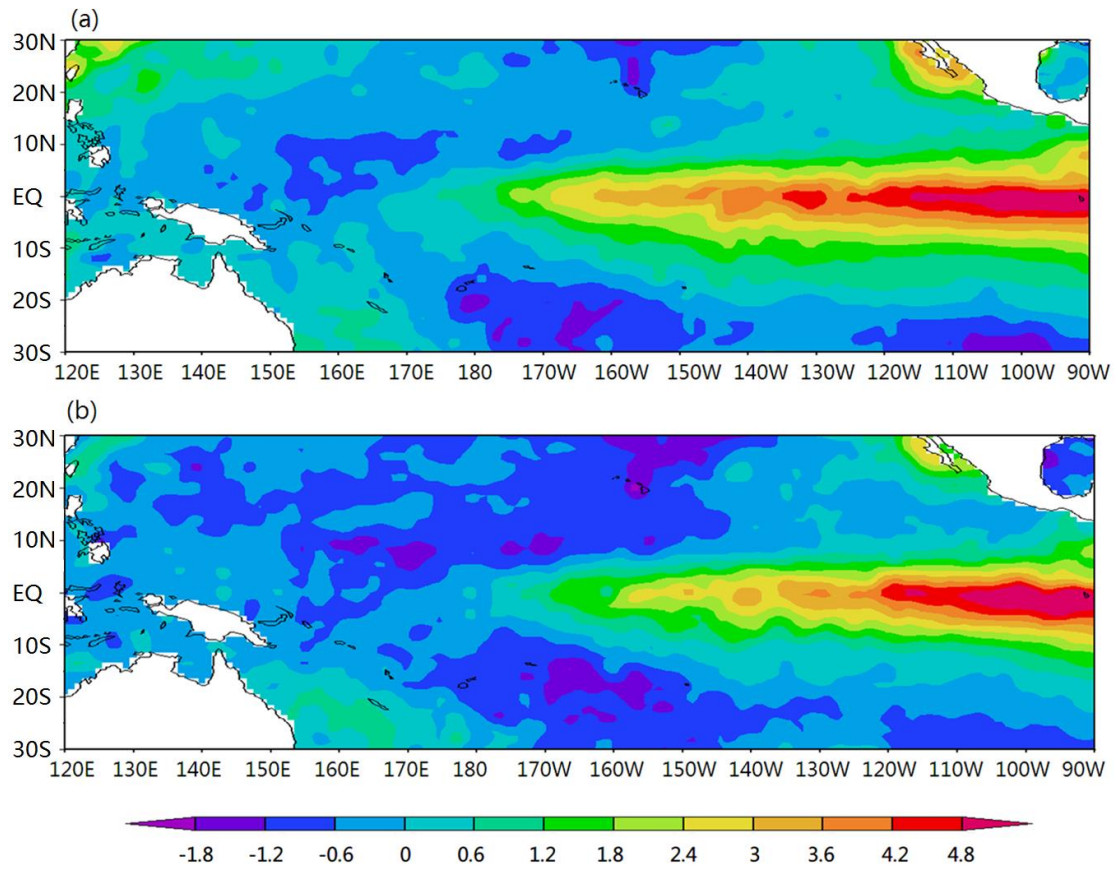
1120

1121

1122

1123

1124



1125

1126 Fig.6. The forecast SSTA field(a) and the actual SSTA field (b)of an El Niño event (Dec.1997)

1127

1128

1129

1130

1131

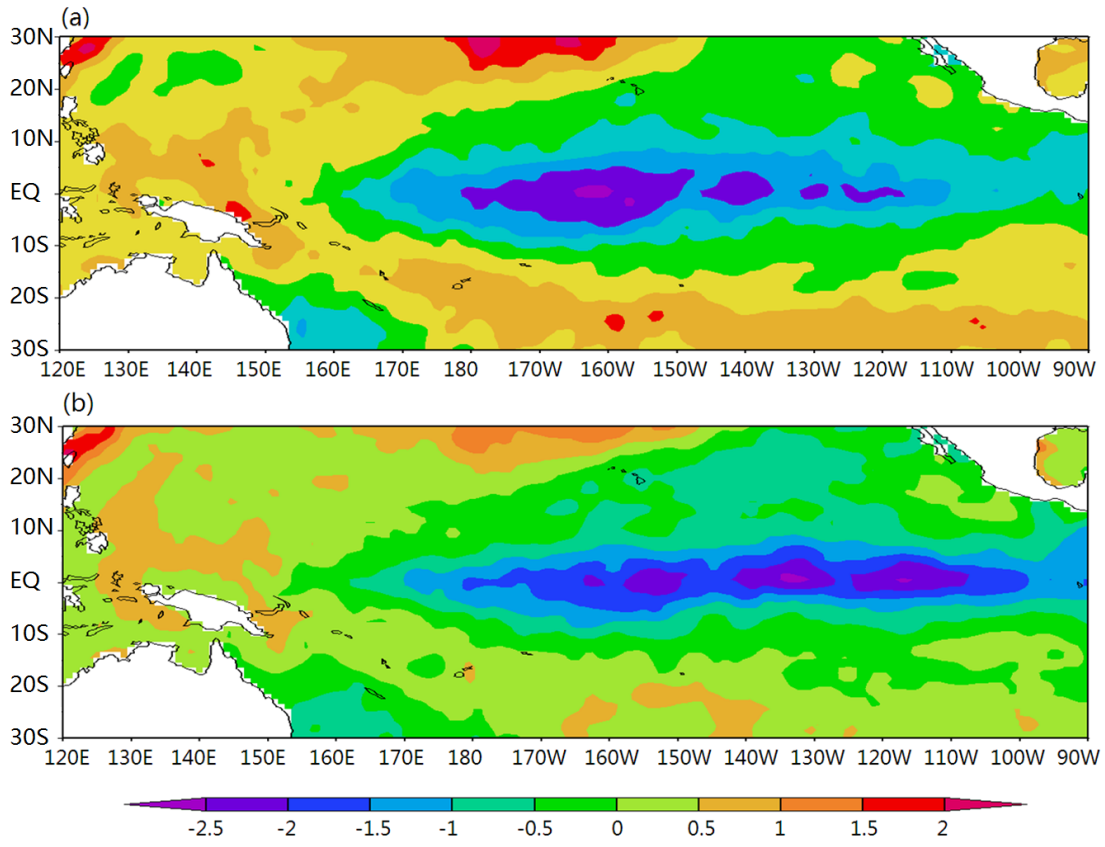
1132

1133

1134

1135

1136



1137

1138 Fig.7. The forecast SSTA field(a) and the actual SSTA field (b)of a La Niña event (Dec.1999)

1139

1140

1141

1142

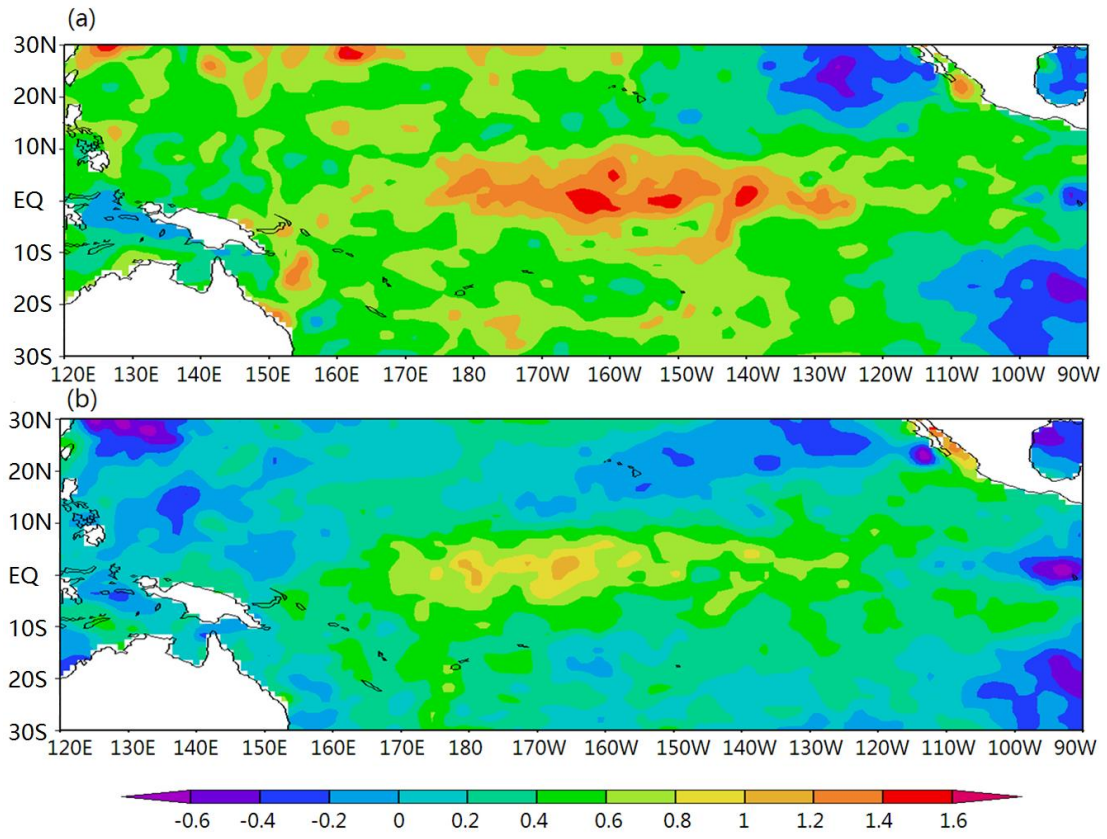
1143

1144

1145

1146

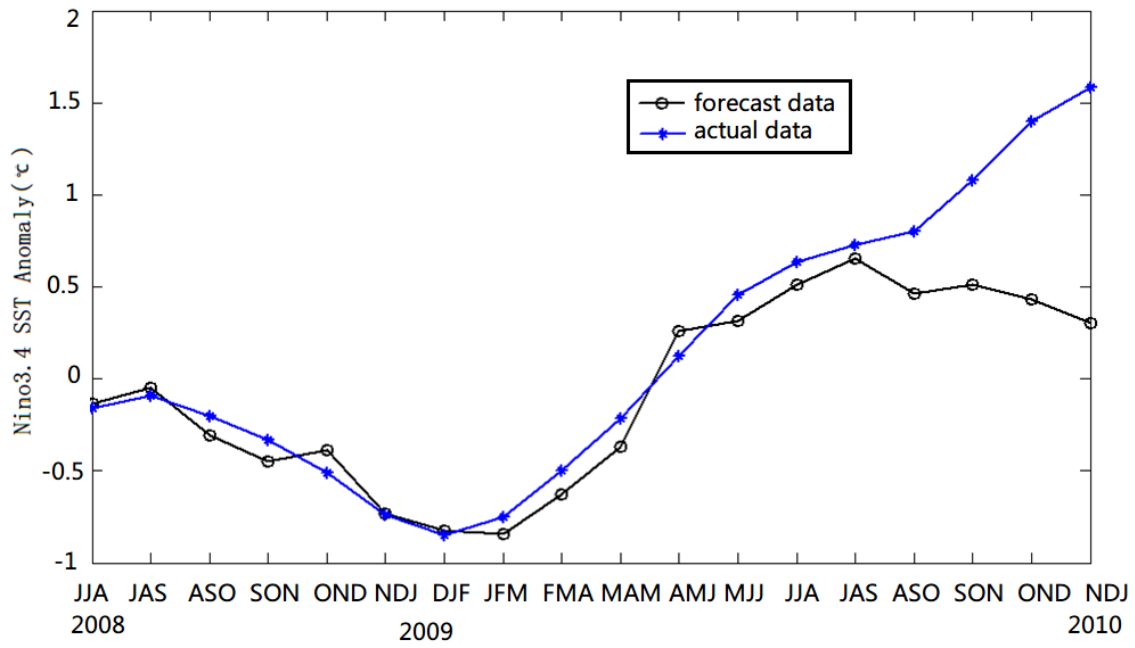
1147



1148

1149 Fig.8. The forecast SSTA field(a) and the actual SSTA field (b)of neutral event (Nov.2002)

1150



1151

1152

Fig.9. The improved dynamical-statistical model prediction of the ENSO index

1153

1154

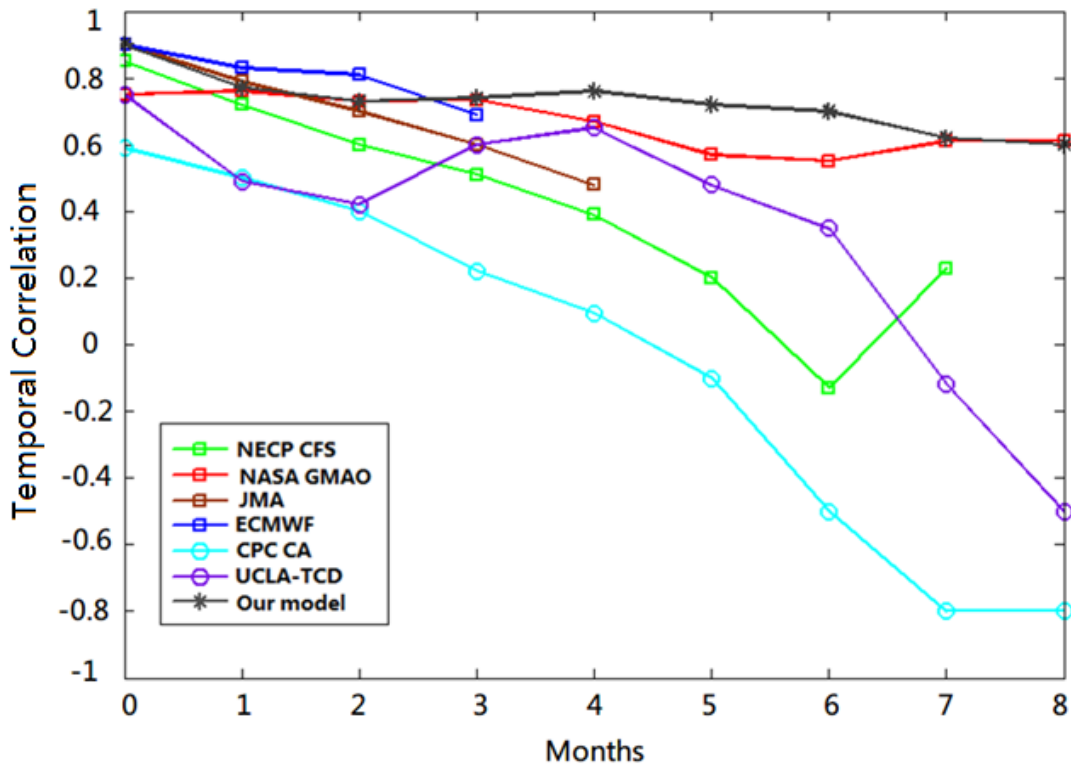
1155

1156

1157

1158

1159



1160

1161 Fig. 10. Temporal correlation between model forecasts and observations for all seasons combined, as a
 1162 function of lead time. Each line highlights one model.

1163

1164

1165

1166

1167

1168

1169

1170

1171

1172

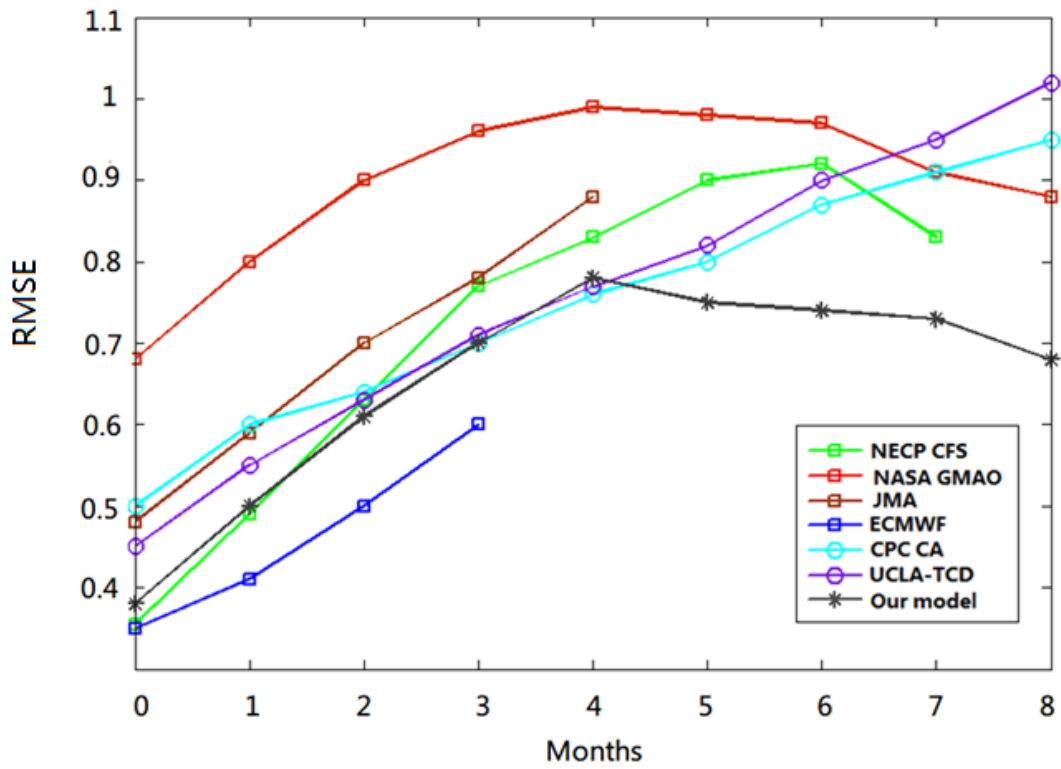
1173

1174

1175

1176

1177



1178

1179

Fig . 11. RMSE in standardized units, as a function of lead time for all seasons combined. Each line

1180

highlights one model.

1181

1182

1183

1184

1185

1186

1187

1188

1189

1190

1191

1192

1193

1194

1195 **Table:**

1196 Table 1. The correlation analysis between the front two time series T_1, T_2 and nine impact factors

factors	u_1	u_2	PNA	DMI	SOI	PDOI	EAWMI	OLR	SSH
T_1	0.3161	0.5684	0.4386	-0.3457	0.7734	0.4081	0.6284	0.3287	0.3363
T_2	0.2118	0.4181	0.2560	-0.2345	0.5232	0.3065	0.4825	0.1816	0.2169

1197

1198

1199

1200

1201

1202

1203

1204

1205

1206

1207

1208

1209

1210

1211

1212

1213

1214

1215

1216

1217

1218

1219

1220

1221

1222

1223

1224

1225

1226

1227

1228

1229

1230 **Table2.** The CC and MAPE of long-term fitting test when the retrospective order p is different

p		4	5	6	7	8	9	10
The forecast results of long-term fitting test	CC	0.75	0.73	0.81	0.74	0.70	0.72	0.68
	MAPE	18.42%	19.36%	14.56%	20.39%	25.31%	24.18%	27.33%
p		11	12	13	14	15	16	
The forecast results of long-term fitting test	CC	0.68	0.70	0.65	0.62	0.60	0.62	
	MAPE	28.10%	26.58%	30.91%	33.14%	34.97%	33.56%	

1231

1232

1233

1234

1235

1236

1237

1238

1239

1240

1241

1242

1243

1244

1245

1246

Table3. The forecast results of T_1 and T_2 in different examples within 6 and 12 months

1247

Forecast events	The results within 6-months		The results within 12-months	
	CC	MAPE	CC	MAPE
The average of 18 El Niño examples of T_1	0.824	8.45%	0.719	12.67%
The average of 22 La Niña examples of T_1	0.846	7.68%	0.740	11.28%
The average of 20 Neutral examples of T_1	0.885	6.23%	0.789	9.85%
The average of total 60 examples of T_1	0.850	7.41%	0.748	10.95%
The average of 18 El Niño examples of T_2	0.811	8.79%	0.703	13.28%
The average of 22 La Niña examples of T_2	0.833	7.35%	0.731	11.96%
The average of 20 Neutral examples of T_2	0.896	6.68%	0.795	10.08%
The average of total 60 examples of T_2	0.842	7.64%	0.740	11.71%

1248

1249

1250

1251

1252

1253

1254

1255

1256

1257

1258 **Table 4.** The TC and the MAPE between model forecasts and observations within 12 months for
 1259 Nov.–Jan., Dec.–Feb., and Jan.–Mar. as lead time of winter, for Feb.–Apr. , Mar.–May and Apr.–June as
 1260 lead time of spring, for May-July, June-August and July-Sep. as lead time of summer and for
 1261 August-Oct., Sep.-Nov. and Oct.-Dec. as lead time of autumn.

Forecast events	Lead time of all seasons combined		Lead time of summer (MJJ-JJA-JAS)		Lead time of autumn (ASO-SON-ON D)		Lead time of winter (NDJ-DJF-JF M)		Lead time of spring (FMA-MAM-AM J)	
	TC	MAPE	TC	MAPE	TC	MAPE	TC	MAPE	TC	MAPE
The average of 18 El Niño examples	0.604	9.70%	0.569	10.33%	0.632	8.85%	0.677	8.02%	0.538	11.6%
The average of 22 La Niña examples	0.625	8.97%	0.581	9.82%	0.645	8.41%	0.695	7.83%	0.579	9.82%
The average of 20 Neutral examples	0.798	5.96%	0.752	6.86%	0.831	5.31%	0.844	4.60%	0.765	7.07%
The average of total 60 examples	0.712	7.62%	0.633	8.51%	0.786	6.88%	0.776	6.52%	0.653	8.03%

1262

1263

1264

1265

1266

1267

1268

1269

1270

1271

1272

Table5. The forecast results of the different data periods

Forecast events	The data periods (Jan. 1951-Dec.2010) Lead time of all seasons combined		The data periods (Jan. 1931-Dec.2010) Lead time of all seasons combined		The data periods (Jan. 1941-Dec.2010) Lead time of all seasons combined		The data periods (Jan. 1961-Dec.2010) Lead time of all seasons combined		The data periods (Jan. 1971-Dec.2010) Lead time of all seasons combined	
	TC	MAPE	TC	MAPE	TC	MAPE	TC	MAPE	TC	MAPE
The average of 18 El Niño examples	0.604	9.70%	0.683	9.02%	0.642	9.35%	0.572	10.15%	0.551	10.44%
The average of 22 La Niña examples	0.625	8.97%	0.701	8.33%	0.675	8.55%	0.589	9.42%	0.567	9.82%
The average of 20 Neutral examples	0.798	5.96%	0.845	5.12%	0.821	5.56%	0.746	6.21%	0.721	6.58%
The average of total 60 examples	0.712	7.62%	0.771	7.14%	0.740	7.38%	0.680	7.96%	0.652	8.15%

1273

1274

1275